



School of Chemistry

Metal-Oxygen Surface Coatings on Doped Diamond for Thermionic Emission

Roger Seddon

April 2018

**This thesis is submitted in partial fulfilment of the requirements for the
Honours Degree of MSci at the University of Bristol.**

Supervisor: Dr Neil Fox

Second Assessor: Prof. Paul May

Section: Physical and Theoretical

Abstract

Direct thermal to electrical energy conversion from thermionic energy converters could be a source of clean power in the future. It is thought that diamond has the physical properties to be the material upon which the devices could be built. However, as of yet, thermionic emission from diamond is inefficient despite its thermal stability. This project looked to find a stable coating which forms an effective negative electron affinity (NEA) surface on doped diamond to enhance its ability thermionically emit electrons.

Metal oxygen based coatings were deposited onto both nitrogen doped and boron doped diamond samples, before the surfaces were characterised using X-ray Photoelectron Spectroscopy (XPS) and their thermionic emission properties were tested. The variations we looked at were in the termination of the diamond before metal deposition (hydrogen or oxygen), the metal used (Ag + Li, Sn + Li, Li), the effect of step annealing under vacuum on the coating thickness, the alloying of multiple metals, and the degree of coverage of the deposited metal.

The effect of termination on the stability of lithiated metal coatings was shown to be that the most stable coatings were on oxygen terminated diamond. Step annealing was shown in all cases to remove metal oxide from the surface but leave metal in place. Lithium on oxygen terminated surfaces was shown to form a NEA surface after annealing to 800 °C for 30 minutes, which was stable up to *ca.* 950 °C. Lithiated silver was shown to not form a NEA surface at the temperatures tested. Lithiated tin was shown to have similar characteristics to the solely lithium coated samples, although thermionic properties are not yet established. The degree of coverage on lithiated silver samples was shown to have little effect.

A lithium oxygen coating has the potential to form a NEA surface on diamond, but the stability and ideal thickness of the coating still require further research to optimise.¹ From this project a less than full monolayer of lithium oxide on the diamond surface was shown to have the lowest work function. There is also scope for other lithiated metal coatings such as titanium or antimony to enhance the thermionic emission of diamond which should be investigated.

Acknowledgements

Dr Neil Fox

Gary Wan

Alex Croot

Dr Mattia Cattelan

UoB Diamond Group

Contents

Abstract.....	1
Acknowledgments.....	2
Contents.....	3
1 Introduction	
1.1 Thermionic Emission.....	4
1.2 Thermionic Energy Converters	
1.2.1 Theory.....	5
1.2.2 Applications.....	6
1.2.3 Caveats.....	7
1.3 History of Diamonds and their Synthesis	
1.3.1 Physical Properties and Early Synthesis.....	9
1.3.2 Chemical Vapour Deposition Synthesis.....	10
1.4 The Doping of CVD Diamond	
1.4.1 Doping Background.....	11
1.4.2 P-Type Doping.....	12
1.4.3 N-Type Doping.....	12
1.4.4 Annealing.....	13
1.5 Surface Termination	
1.5.1 The Diamond Surface.....	13
1.5.2 Negative Electron Affinity Surfaces.....	14
1.5.3 Schottky Junctions and Diodes.....	15
2 Experimental	
2.1 Aims.....	16
2.2 Equipment.....	16
2.2.1 Sample Preparation.....	16
2.2.2 Sample Analysis.....	20
2.3 Methodology	
2.3.1 Material Selection.....	21
2.3.2 Annealing and Characterisation.....	22
3 Results and Discussion	
3.1 Hydrogen and Oxygen Terminations.....	24
3.2 Silver/Lithium.....	25
3.3 Lithium/Oxygen.....	28
3.4 Tin/Lithium.....	31
3.5 Caveats.....	35
4 Conclusions	
4.1 Summary.....	37
4.2 Future Work.....	38
5 Bibliography	40

1 Introduction

1.1 Thermionic Emission

The phenomenon of thermionic emission has been observed for over 160 years, although an understanding of the phenomenon is somewhat more recent. It has been reported and rediscovered by many famous names over the years including Edmond Becquerel and Thomas Edison.^{2,3} However, it was Owen Richardson who proposed the theory that is still widely accepted, and in doing so he coined the term ‘thermionic emission’ and won the 1928 Nobel Prize in Physics. The most widely observed phenomenon was that of lamp filaments breaking and incandescent lamps blackening more intensely near their positive terminals. Richardson’s explanation for this was that the heating of a material can excite electrons to overcome the material’s work function and be expelled.⁴ This can be described mathematically using the Richardson-Dushman equation,

$$J = A_G T^2 e^{\frac{-\varphi}{kT}}, \quad (1)$$

where J is the emission current density ($A\ m^{-2}$), A_G is the Richardson constant, T is the temperature of the emitting material (K), φ is the work function of the emitting material (J), and k is the Boltzmann constant ($J\ K^{-1}$).⁵

The true value of A_G is still the object of academic debate today, although A_G is agreed to be in the form of,

$$A_G = \lambda_R A_0. \quad (2)$$

Where λ_R is a material specific correction factor and A_0 is a universal constant defined by,

$$A_0 = \frac{4\pi m k^2 e}{h^3}, \quad (3)$$

and has a value of $1.20173 \times 10^6\ A\ m^{-2}\ K^{-2}$ with m and e being the mass and charge of an electron, respectively.⁵

The Richardson-Dushman equation is only really valid for metallic surfaces, as such, modifications need to be made to it for it to be valid for semi-conducting materials. The erroneous assumption made is that the electrons to be emitted are delocalised and therefore can be treated with bulk kinetic theory, however, for wide bandgap materials such as doped diamond, this is not the case. Another

assumption made is that the density of states scales as $e^{1/2}$, which is true for a highly conductive metal, but for a semi-conductor with a bandgap, this cannot be true. λ_R is a suitable correction, for wide bandgap materials the correction decreases the value of the Richardson constant.⁶

Thermionic emission can be enhanced by giving the emitter a negative bias, which creates an electric field local to the emitting surface. The presence of the electric field can lower the work function of the emitter.⁷ This effect is known as the Schottky effect after the physicist Walter H. Schottky and can be defined by a modified Richardson-Dushman equation,

$$J = A_C T^2 e^{\frac{-(\phi - \Delta\phi)}{kT}}. \quad (4)$$

Where $\Delta\phi$ is the change in barrier height induced by the electric field,

$$\Delta\phi = \sqrt{\frac{e^3 F}{4\pi\epsilon_0}}, \quad (5)$$

where F is the magnitude of the electric field (V m^{-1}) and ϵ_0 is the vacuum permittivity ($8.854 \times 10^{-12} \text{ F m}^{-1}$).⁷

1.2 Thermionic Energy Converters

1.2.1 Theory

The heating of a thermionic emitters releases electrons out of the material which can then be collected and used to generate current. If a cold collector for high energy emitted electrons is placed across a small vacuum gap from the hot emitter and there is a circuit connecting them, a charge difference is created so a resulting current will flow (see figure 1). This is the basis of thermionic energy conversion.

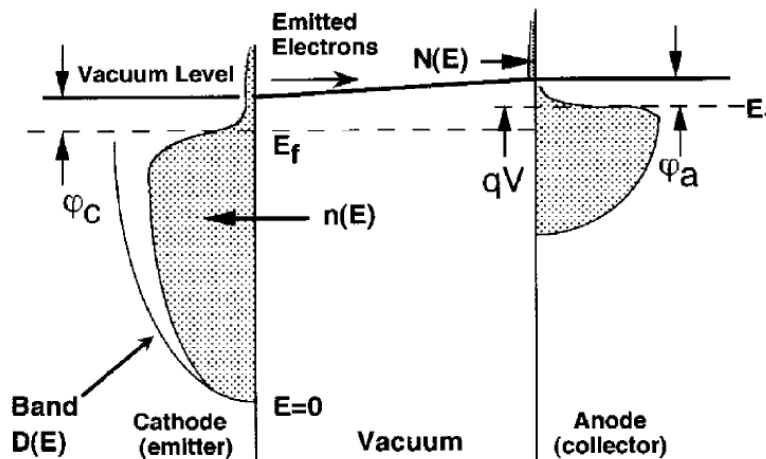


Figure 1. Energy band diagram for the electrodes of a thermionic energy converter.⁸

For a thermionic energy converter (TEC) to work there is usually high or ultra-high vacuum between the electrodes, otherwise the electrons would likely not reach the collector. Not only does the vacuum increase the collection probability, but it also helps insulate the two electrodes from each other. This insulation is important as it helps to maintain the temperature differential between the electrodes which is essential for maximising the Carnot cycle efficiency (η_{carnot}) of the system; TECs being a thermodynamic engine converting heat into work. TECs represent a way of converting heat into work without any intermediary steps required, this could be massively more efficient than current methods of energy generation such as the steam turbines used in fossil fuel fired power stations which linger at 40-50 %.⁹

1.2.2 Applications

The first serious application of TECs was for powering satellites launched by the USA and Soviet Union during the space race of the 1960s. These set-ups relied on thermal energy from nuclear power, *e.g.* the *TOPAZ* reactor used by the Soviets for powering satellites in the early 1970s used uranium as fuel.¹⁰ However, due to factors such as unreliability and cost, this style of reactor was superseded for extra-terrestrial use by thermoelectric generation technologies like the radioisotope generator *Orion 1* used by the Soviet Union.¹¹ Other contributing factors for diminishing research in thermionic converters in the late 20th century was the cessation of the space race and the fall of the Soviet Union, and the advent of effective photovoltaic cells.

The photovoltaic cells that had themselves superseded thermionic reactors could, however, be a potential area that TECs could improve. Photovoltaic cells work by implementing the photovoltaic effect whereby a material (usually a semiconductor) absorbs a photon which excites an electron. The aspect that TECs could help with is that the absorbed photon is seldom of the correct wavelength to have the same energy as the bandgap, meaning that when photons have sufficient quanta and are absorbed, any excess energy is lost as heat. Naturally if the energy lost as heat could be converted to work, the system would be more efficient. Photon-enhanced thermionic emission (PETE) exploits exactly this to minimise thermalisation loss by working photovoltaic absorption and thermionic emission in tandem.¹² This technique, although not perfect has been shown to improve the efficiency of solar cells by up to 17 %.¹³ The main drawback of PETE is that the

thermionic system has to operate at temperatures double that of the upper limit of most silicon based solar cells.

1.2.3 Caveats

TECs have several drawbacks for which solutions are being intensively researched before the technology can become more widespread. First of all, finding suitable materials for the emitting and collecting electrodes is challenging. The materials must both be thermally stable at a wide range of temperatures, the emitter must be semi-conducting, and both must have low work functions, whilst maintaining a large work function difference between electrodes (the emitter's must be at least 1 eV higher than the collector's).¹⁵ Examples of known, valid materials are phosphorous doped polycrystalline diamond, polycrystalline silicon carbide, and nitrogen doped nanodiamond films on silicon substrates. Finding increasingly more suitable materials is largely a trial and error problem, however modifications can be made to existing electrodes to reduce their work function. The surface of the semiconductor can be given a coating of an electropositive material to create a negative electron affinity (NEA), which has been shown to reduce the work function of materials, *e.g.* a deposition of potassium in an oxidant atmosphere onto p-type silicon reduced its work function from 4.7 eV to 1.35 eV.¹⁶ The intercalation of materials such as alkali metals into the semi-conductor can also reduce its work function.¹⁷ Another consideration when assessing the suitability of new materials is the field emission properties of the emitter, *i.e.* how likely the material is to emit electrons in the presence of an electrostatic field. Field emission can enhance thermionic emission by lowering the Schottky barrier. Non-planar surface structures can induce a local electric field thus inducing field emission enhanced thermionic emission (see figure 2).

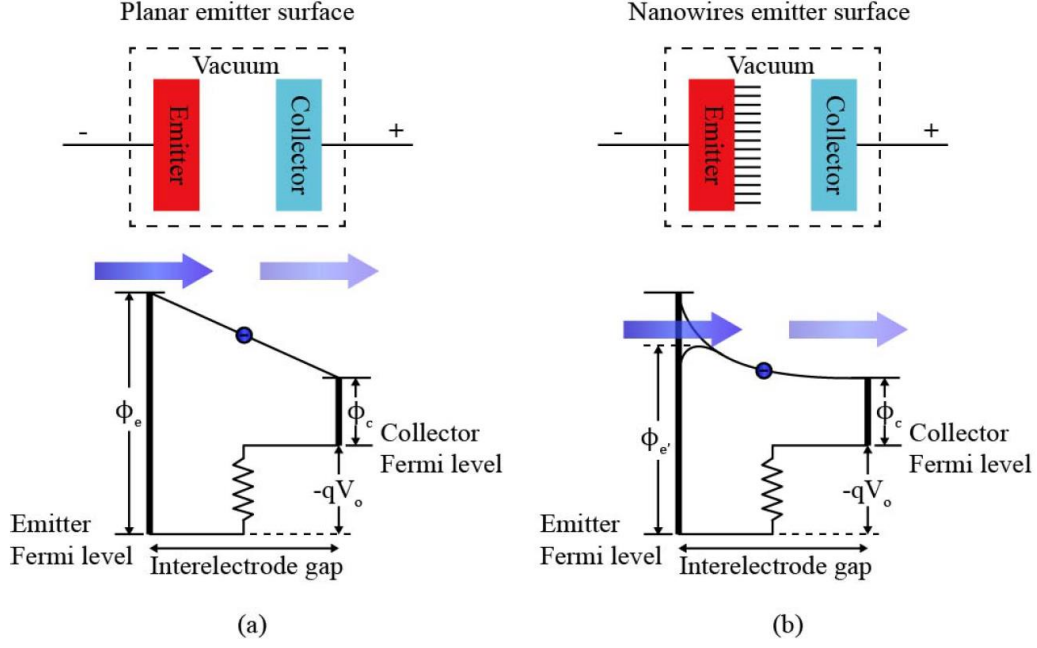


Figure 2. A demonstration of the reduced work function due to surface nanostructures.¹⁴

The other main drawback is the formation of space charge clouds in the vacuum between the electrodes. The space charge is in essence the problem of low energy emitted electrons being attracted back towards the positively charged emitter forming a cloud, which in turn repels further low kinetic energy electrons, preventing them from reaching the collector due to the formation of an increasingly negative barrier to overcome. Two methods are used for negating the space charge, reducing the interelectrode distance or the *in situ* neutralisation of the electron cloud, both of which have drawbacks. Reducing the interelectrode distance reduces the kinetic energy an electron requires to reach the collector by reducing the interelectron collision frequency. The major drawback is the increased thermal transfer reducing the Carnot efficiency of the system, with the Carnot efficiency defined as,

$$\eta_{carnot} = 1 - \frac{T_{cold}}{T_{hot}}. \quad (6)$$

A balance must therefore be struck between reduction of space charge and the increase of thermal transfer, for which radiative transfer increases exponentially with shorter distance.¹⁸ It has been found that an ideal interelectrode gap is between 0.9 and 3 μm , but depends on the energy of the thermal radiation.¹⁹ However, such tiny gaps are seldom used due to the difficulty of such small dimensions and the required tolerances.

1.3 History of Diamonds and their Synthesis

1.3.1 Physical Properties and Early Synthesis

Since the late 18th century, the superlative properties of diamond have led it to become the foremost gem. Diamond is remarkable in that for a bulk material it has the highest thermal conductivity (20 W cm^{-1}) at room temperature, the highest Young's modulus (1100-1170 GPa depending on surface), the highest hardness (10 on the Mohs scale), and an ultrawide-band optical transmission range (from 220 nm to the far IR and including some radio and microwave frequencies).^{20,21,22,23} These properties have led to a great amount of research into the synthesis of diamond in laboratories, as previously diamonds had to be mined in places such as India and Southern Africa. Despite valiant attempts in the late 19th century by both J. B. Hannay and Henri Moissan, it is accepted that the first successful synthesis of diamond was not carried out until 1955 by H. Tracy Hall working for General Electric.^{24,25,26,27} The conditions that Hall used have become known as 'high-pressure, high-temperature' (HPHT) conditions, in the initial case graphite was exposed to temperatures of between 1,000 – 3,000 K and pressures between 30,000 – 100,000 kg cm^{-2} .²⁷ These conditions are similar to those under which diamonds were originally created in the Earth's core, at which point the sp^2 carbon in graphite is converted into sp^3 diamond (see figure 3). When this technology was in its infancy, the largest synthetic diamonds that could be produced were of the order of one quarter of a carat, to this end, their widespread use in industry could not reach its full potential.

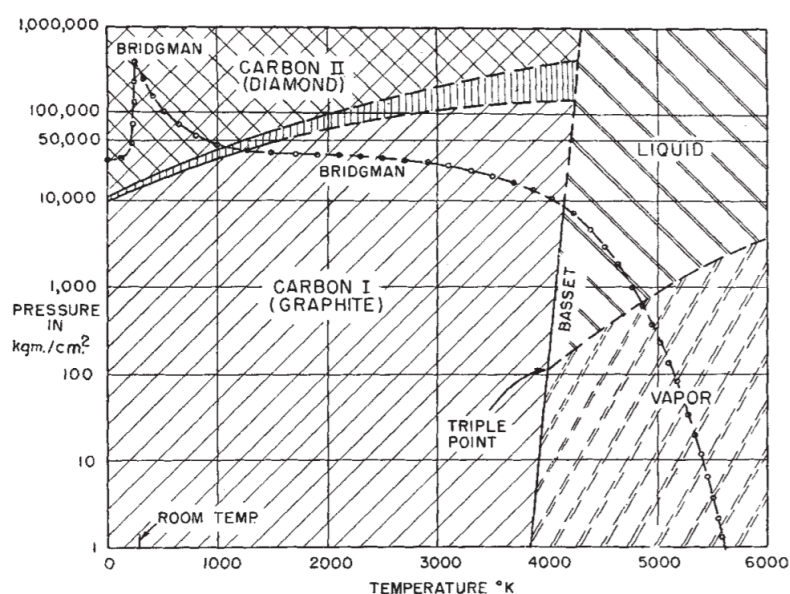


Figure 3. The phase diagram of carbon.²⁷

1.3.2 Chemical Vapour Deposition Synthesis

With increased industrial exploitation in mind, new synthetic methods were sought with great zeal. The main product of this is the chemical vapour deposition (CVD) synthesis of diamond. The two main methods of CVD, hot-filament (HFCVD) and microwave-plasma (MWCVD), were first successfully carried out in the early 1980s by Seiichiro Matsumoto's group and Mutsukazu Kamo's group respectively, both working at NIRIM in Japan.^{28,29} Both techniques have similar mechanisms, but use different methods of radicalisation. The process is usually carried out in pressures of between 20 and 100 Torr of a gaseous mixture of highly pure H₂ and a hydrocarbon (usually methane) on a substrate which can readily react with carbon, such as molybdenum or silicon, in addition these substrates can be seeded. At high temperatures (caused either by a filament or a microwave induced plasma), the gases are radicalised and then hydrogen radicals can sequester hydrogen atoms from the surface of the substrate, leaving a radical carbon at the surface which can then react with a CH₃ radical to form the C-C sp³ bond needed for diamond growth, with dangling CH₃ groups being radicalised and reacting with each other to form the sp³ lattice structure. See figure 4.

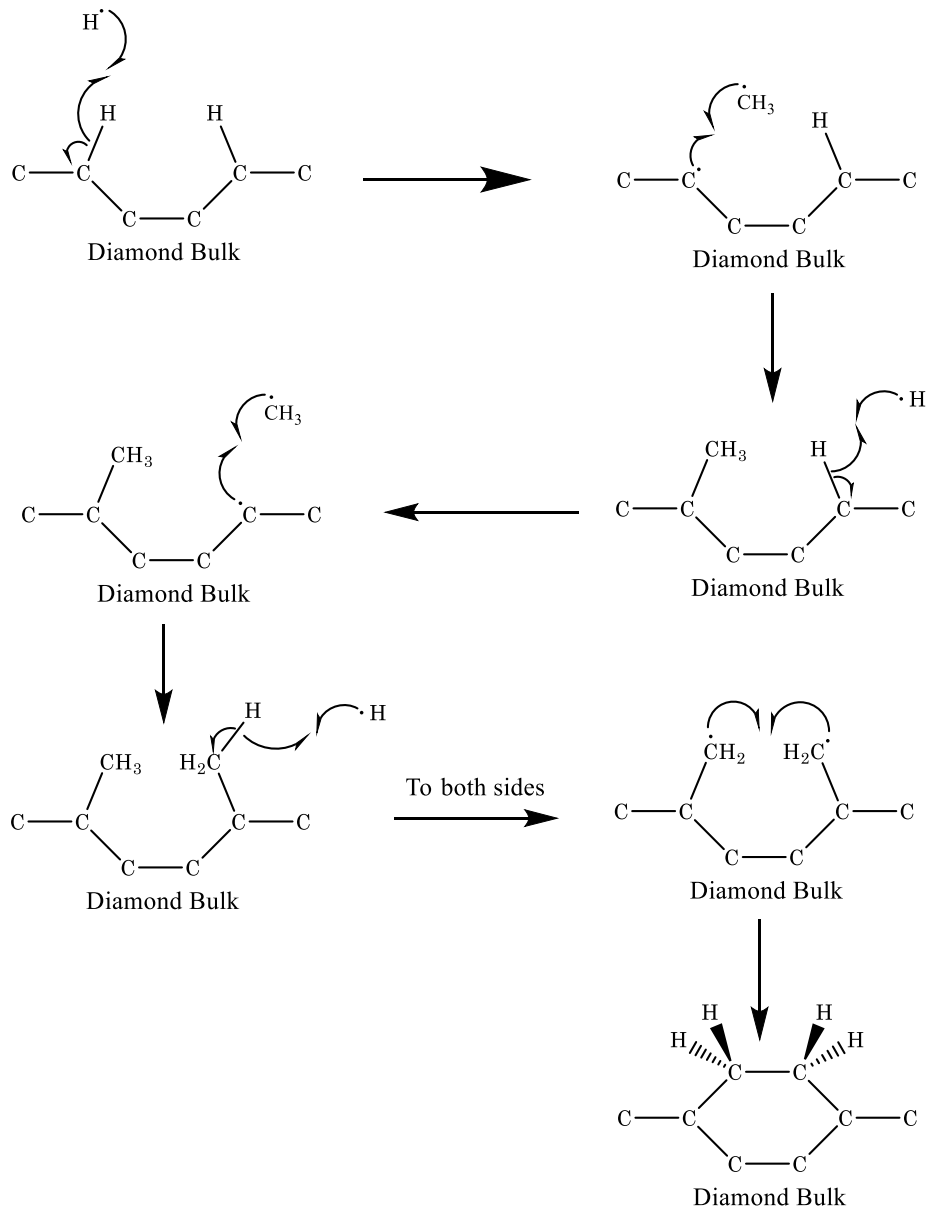


Figure 4. Proposed CVD surface diamond growth mechanism.³⁰

1.4 The Doping of CVD Diamond

1.4.1 Doping Background

The optical and electronic properties of diamond can be tuned by introducing impurities into the lattice structure. This doping can easily be done when growing CVD diamond; one simply introduces the desired dopant into the reaction atmosphere as the growth is occurring. The resulting doped diamond will have a relatively evenly distributed impurity of a desired concentration.

The electronic (and therefore optical) properties of diamond derive from its band gap, which for high purity diamond is wide at 5.48 eV.³¹ This band gap equates to a wavelength of 225 nm which is in the UV part of the spectrum. However, when impurities are introduced the electronic structure is changed and the diamond can absorb in the visible part of the spectrum, for example boron doped diamond appears blue and nitrogen doped diamond appears yellow. The scope of elements with which one can dope diamond is small due to the constraints of having such a strong lattice and maintaining the sp^3 nature of the carbons atoms; usually one of boron (p-type), nitrogen or phosphorus (n-type), and sometimes hydrogen is used, see figure 5.

1.4.2 P-Type Doping

P-type acceptor doping works by creating an electron hole in the lattice, in diamond this happens when using boron because boron has only 3 valence electrons so can only form three bonds. Thus, one of its neighbouring sp^3 carbons will have an unbonded electron. The result of this is that the Fermi level is reduced to 0.37 eV above the valence band, a deep acceptor level.³² Boron fits well into the lattice because its covalent radius of 0.84 Å is just 0.08 Å larger than carbon's.^{33,34}

1.4.3 N-Type Doping

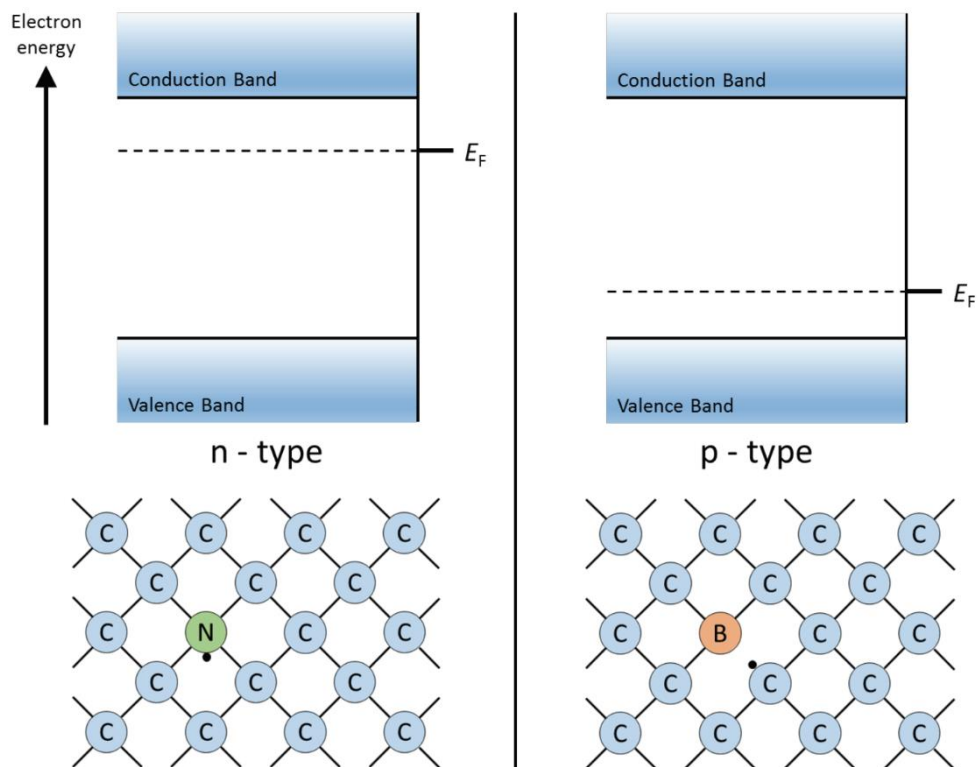


Figure 5. Diagram of p and n-type doped diamond, and their band structures.³⁵

N-type donor doping works in the opposite manner, as the name suggests it causes the lattice to have extra electrons. A commonly used n-type dopant is nitrogen which also fits well into a sp^3 carbon lattice with a covalent radius of 0.71 Å.³⁴ Nitrogen has 5 valence electrons so makes four bonds with its neighbouring sp^3 carbons leaving one unbonded electron on the nitrogen. The resulting band structure of nitrogen doped diamond is a raised Fermi level which sits 1.7 eV below the conduction band.³² From this high Fermi level electrons can be easily promoted into the conduction band. An even higher Fermi level can be achieved by doping with phosphorus (0.57-0.62 eV below the conduction band), although, due to its size, phosphorus doping has to be done largely on [111]-oriented substrates, a rather unorthodox method and difficult to perform with diamond.³²

1.4.4 Annealing

Annealing is an important process in the doping process, especially if the doping is for electronic properties. Annealing gives the lattice a more even distribution of dopants. For example, annealing a boron doped diamond sample at 900 °C in an He ambient increases the number of substitutional boron atoms and changes the electronic properties to have more ohmic character, and its 2.4 eV emission is greatly intensified.³⁶

1.5 Surface Termination

1.5.1 The Diamond Surface

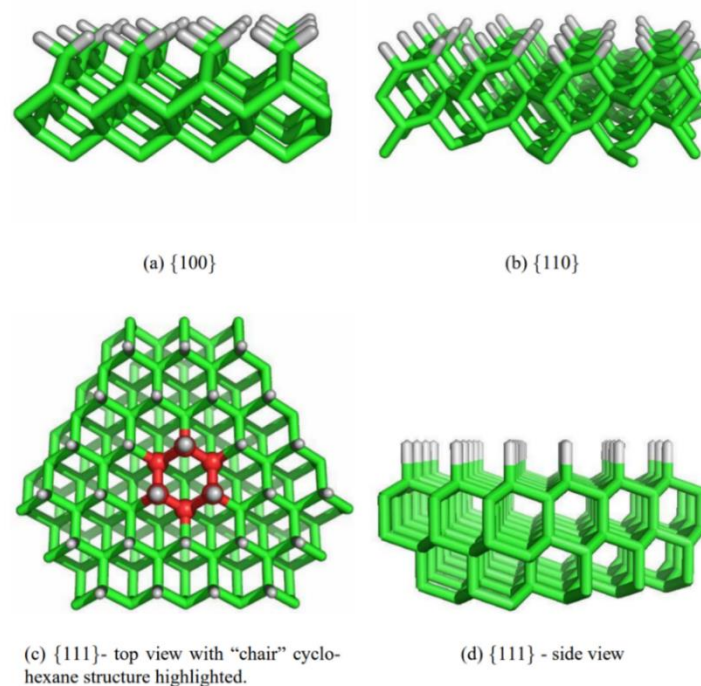


Figure 6. Diamond surface morphologies with hydrogen termination.³⁷

The diamond lattice has twofold, fourfold, and sixfold symmetry represented by the primary planes [100], [110], and [111] respectively (see figure 6). The surfaces on these planes differ in terms of protruding atoms and dangling bonds, [100] has two dangling sp^3 bonds and both [110] and [111] have just one, which are inherently unstable. To provide stability the surface structure is altered from the bulk structure in terms of hybridisation or by being terminated with heteroatoms by chemisorption. This termination mimics the form of organic molecules with carbon-hydrogen or carbon-oxygen bonds, enabling the top carbons to retain their sp^3 hybridisation. When hydrogen terminated the surface would appear to uniformly have aliphatic carbon-hydrogen bonds. However, when oxygen terminated, several forms of bond are apparent: ether, ketone, and peroxy.³⁸ The ether form has a half monolayer of one oxygen bridging two sp^3 hybridised carbons (C-O-C), whereas the ketone has a monolayer of one oxygen per carbon with a double bond between them (C=O), making the carbon sp^2 hybridised. These two forms occur at the [100] surface. A peroxy bridge form is proposed of the form C-O-O-C is also proposed for the [111] single bond cleavage surface.³⁹

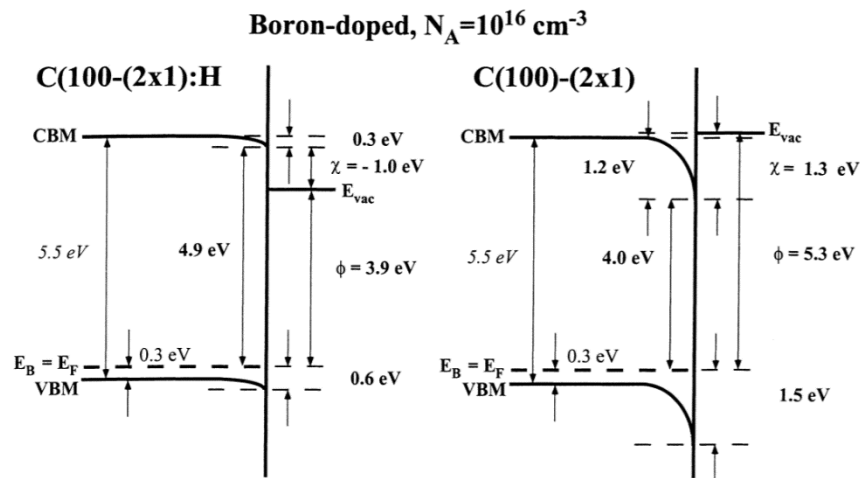


Figure 7. Work function reduction for p-type diamond after hydrogen termination.⁴⁰

1.5.2 Negative Electron Affinity Surfaces

The termination of the diamond can be exploited to enhance certain properties, like the aforementioned NEAs. For hydrogen terminated diamond, the way the NEA is thought to work is through the creation of a dipole at the surface along the C-H bond with hydrogen being more electropositive than carbon. Because of the dipole, the energy level of the vacuum level is lowered to below the minimum of the conduction band, see figure 7.⁴¹ With a band structure as such and with band bending factored in, the electron affinity of the surface can be negative. The result

of this is that it is much easier for electrons that have been excited into the conduction band to be emitted from the material. Hydrogen is classed as a true NEA and it is the most effective NEA known at present, however it is unstable at high temperatures, it will completely desorb from nitrogen doped polycrystalline CVD diamond above 750 °C. Besides hydrogen, NEA surfaces can be achieved with thin depositions of alkali metals such as lithium and potassium on a bare or oxygenated surface. These, however, are classed as effective NEAs as the vacuum level will only be lower than the conduction band minimum because of the band bending caused by the Fermi level being raised to the metal diamond interface.¹

Positive electron affinity surfaces are also possible when the terminating heteroatoms are more electronegative than carbon. A chief example of this is oxygen terminated carbon. These surfaces hinder the emission of electrons by as the dipole across the terminating bond gives the carbon lattice the positive pole.⁴²

1.5.3 Schottky Junctions and Diodes

The size of work function reduction for one coating also depends on which plane the coated surface lies.⁴³ When metals are directly deposited onto the semiconductor surface the junction can have several advantageous properties. The metal-semiconductor junction, also called a Schottky junction can have the effect of band bending depending on the Fermi levels of the two materials, and these properties form the basis of Schottky diodes. The useful rectifying properties arise when a bias is applied to the system. With a forward bias, excited electrons are able to move from the semiconductor conduction band into the metal, whereas with a reverse bias the barrier for that transfer is too high so electrons cannot pass from the semiconductor to the metal.⁶ A similar phenomenon occurs at the junction of a p-type and an n-type semiconductor.

2 Experimental

2.1 Aims

Basing our research on the work of others at the University of Bristol and groups elsewhere, our aim was to find a stable and effective NEA coating for doped diamond to enhance its ability to thermionically emit electrons. To do this we applied a variety of metal surface coatings to both nitrogen doped and boron doped diamond samples before characterising their surfaces and studying their thermionic emission properties. The variations we looked at were in the termination of the diamond before metal deposition, the metal used, the metal coating thickness, the alloying of multiple metals, the degree of coverage of the deposited metal, and the annealing of the coatings under vacuum.

2.2 Equipment

2.2.1 Sample Preparation

Two types of sample were used for this project, for the p-type samples, commercially available boron doped, freestanding, polycrystalline, CVD diamond was used, specifically Element Six's 10.0mm × 10.0mm × 600 μm with a dopant concentration of between 2 and 6×10²⁰ atoms cm⁻³. For the n-type samples, nitrogen-doped polycrystalline, CVD diamond film on a 0.5 mm thick Mo substrate were used. These were grown by Alex Croot in the University of Bristol Diamond laboratory in 2017 and have specifications of 10mm × 10mm × 1 μm of diamond film with a dopant concentration of between 5×10¹⁹ and 5×10²⁰ atoms cm⁻³. The nitrogen doped samples were grown for 15 minutes with 4% CH₄ and 0.4% N₂ at 900 °C and 130 Torr.

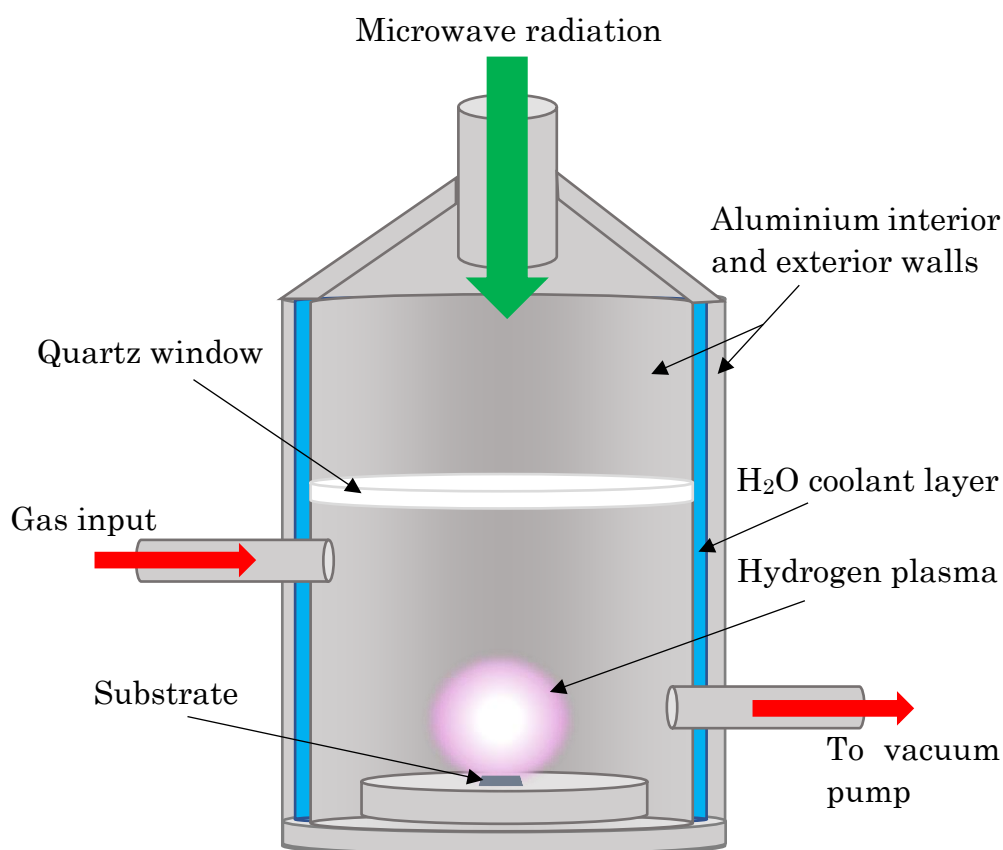


Figure 8. Microwave CVD reactor schematic.

Before metal deposition, all the samples were first hydrogen terminated and then some were oxygen terminated. Hydrogen termination was carried out in a microwave chemical vapour deposition reactor powered by a 1.5 kW ASTeX Magnetron, the plasma was generated using 2.45 GHz microwave radiation, see figure 8. The termination had three phases: cleaning, deposition, and cooling, detailed in table 1. The plasma used was that of pure hydrogen. The first step used a high-energy plasma to ensure the desorption of contaminants from the diamond surface, before lowering the plasma energy to allow the chemisorption of hydrogen onto the vacant sites. After cooling the chamber was evacuated then brought to 500 Torr with Ar gas before being opened to atmosphere.

Hydrogen Termination Conditions

	Cleaning	Deposition	Cooling
Pressure / Torr	85	30	30
Power / Watt	1200	700	0
Hydrogen Flow / sccm	300	300	300
Time / minutes	2	2	2

Table 1. Reactor conditions for the hydrogen termination of 1 cm² CVD diamond samples.

Oxygen termination was carried out by exposing the hydrogen terminated samples to ultraviolet-excited ozone in a Jelight UVO-cleaner for half an hour. With termination complete, the deposition of metal coatings was carried out in a Balzers BA-510 coating chamber. Conditions were as follows:

Silver/lithium film- Samples were mounted upside down on a steel plate in a stainless steel calotte holder and positioned 40 cm from the source boats. A k-type thermocouple was mounted in the coating chamber to record the calotte plate temperature. Pure tungsten dimple boats were mounted for evaporation of silver and lithium from separate boat positions. The coater was pumped overnight for 18 hours to a base pressure of 40 μ Torr. An argon-oxygen gas mixture Ar:O₂ 4:1 was introduced into the chamber using a leak valve to raise the dynamic vacuum pressure to 0.17 Torr. A gas plasma with a current of 70 mA was maintained at a power level of 100 W for 10 minutes. The leak valve was closed, and the vacuum allowed to return to base pressure for 3 hours. Lithium metal was first evaporated to a thickness of approximately 10 nm followed by a silver film of a similar thickness. After deposition the vacuum was broken, and the samples demounted for analysis.

Lithium/tin film- Samples were mounted with a thermocouple as for silver/lithium. Pure tungsten dimple boats were mounted for evaporation of tin and lithium from separate boat positions. The coater was pumped overnight for 18 hours to a base pressure of 40 μ Torr. A current of 3 A was applied to the calotte heater to raise the sample temperature to 120 °C. An argon-oxygen gas mixture Ar:O₂ 4:1 was introduced into the chamber using a leak valve to raise the dynamic vacuum pressure to 0.17 Torr. A gas plasma with a current of 70 mA was maintained at a power level of 100 W for 10 minutes. The leak valve was closed, and the vacuum allowed to return to base pressure for 3 hours. Lithium metal was first evaporated to a thickness of approximately 10 nm followed by a tin film of a similar thickness. After deposition the vacuum was broken, and the samples demounted for analysis.

Oxygen/lithium film 1- Samples were mounted with a thermocouple as for silver/lithium. A pure tungsten dimple boat was mounted for evaporation of lithium from a single boat position. The coater was pumped overnight for 18 hours to a base pressure of 40 μ Torr. A current of 3 A was applied to the calotte heater to raise the sample temperature to 120 °C. An argon-oxygen gas mixture Ar:O₂ 4:1 was introduced into the chamber using a leak valve to raise the dynamic vacuum pressure to 0.17 Torr. A gas plasma with a current of 70 mA was maintained at a power level of 100 W for 10 minutes. The leak valve was closed, and the vacuum allowed to return to base pressure for 3 hours. Lithium metal was evaporated to a thickness of approximately 20 nm. After deposition the calotte heater was switched off and the chamber allowed to cool. Afterwards the vacuum was broken, and the samples demounted for analysis.

Oxygen/lithium film 2- Samples mounted upside down on steel plate in stainless steel calotte holder and positioned 40 cm from source boats. A k-type thermocouple was mounted in the coating chamber to record the calotte plate temperature. Pure tungsten dimple boat was mounted for evaporation of lithium from a single boat position. The coater was pumped overnight for 18 hours to a base pressure of 40 μ Torr. A current of 3.5 A was applied to the calotte heater to raise the sample temperature to 125 °C. An argon-oxygen gas mixture Ar:O₂ 4:1 was introduced into the chamber using a leak valve to raise the dynamic vacuum pressure to 0.17 Torr. A gas plasma with a current of 70 mA was maintained at a power level of 100 W for 10 minutes. The leak valve was closed, and the vacuum allowed to return to base pressure for 3 hours. The deep cooled trap was filled with liquid nitrogen to reduce the base pressure for deposition to reach 8 μ Torr. Lithium metal was evaporated to a thickness of approximately 50 nm. After deposition the calotte heater was switched off and the chamber allowed to cool. Afterwards the vacuum was broken, and the samples demounted for analysis.

For samples where the degree of coverage was changed for the coating, tantalum grids were used, see figure 9. These were prepared from tantalum foil of 50 μ m thickness. The grid pattern was cut using a laser cutter to give varying degrees of coverage, grids of 33%, 50% and 75% Ta coverage were made with individual bars ranging from 5 μ m to 200 μ m. The minimum grid line width was governed by the laser spot size. Grids were attached to the samples using Kapton tape. Tantalum was selected due to its high thermal stability and its relative inertness.

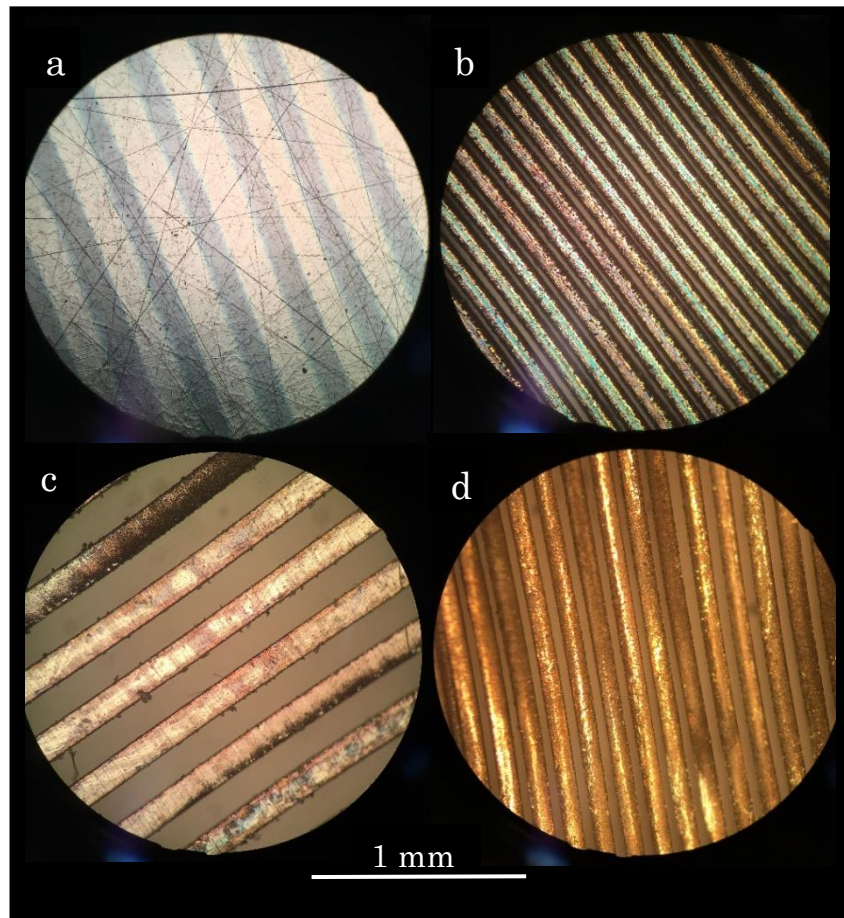


Figure 9. Optical microscope (100× magnification) images of: a) Ag-Li deposited on O-terminated boron doped polycrystalline CVD diamond (66% PVD metal coverage), b) 75% Ta coverage grid, c) 33% Ta coverage grid, d) 50% Ta coverage grid.

For the nitrogen doped diamond samples on molybdenum substrates, 10.6 μm striations were etched with a laser cutter into the molybdenum base. This was done so that the samples could better absorb the IR laser radiation, as molybdenum is a refractory metal. 10.6 μm was chosen as the surface microstructures were of similar dimensions to the wavelength of the incident photons (10.2 – 10.8 μm). These structures allow for surface plasmon polariton excitation, giving more efficient absorption of radiation and therefore heating.⁴⁴

2.2.2 Sample Analysis

Characterisation of the surface coating was carried out by X-ray photoelectron spectroscopy (XPS) in the NanoESCA II facility in the University of Bristol's Centre for Nanoscience and Quantum Information. The NanoESCA II made by Scienta Omicron is an ultra-high vacuum (UHV) system with several surface

analysis functions, the one used was the XPS ARGUS analyser with a resolution of less than 300 meV. Al K α radiation ($h\nu = 1486.7$ eV) was used with a dwell time of 0.5 s and a step size of 0.05 eV. All spectra taken had the probe aimed at the sample at 335° to analyse the bulk, unless otherwise stated.

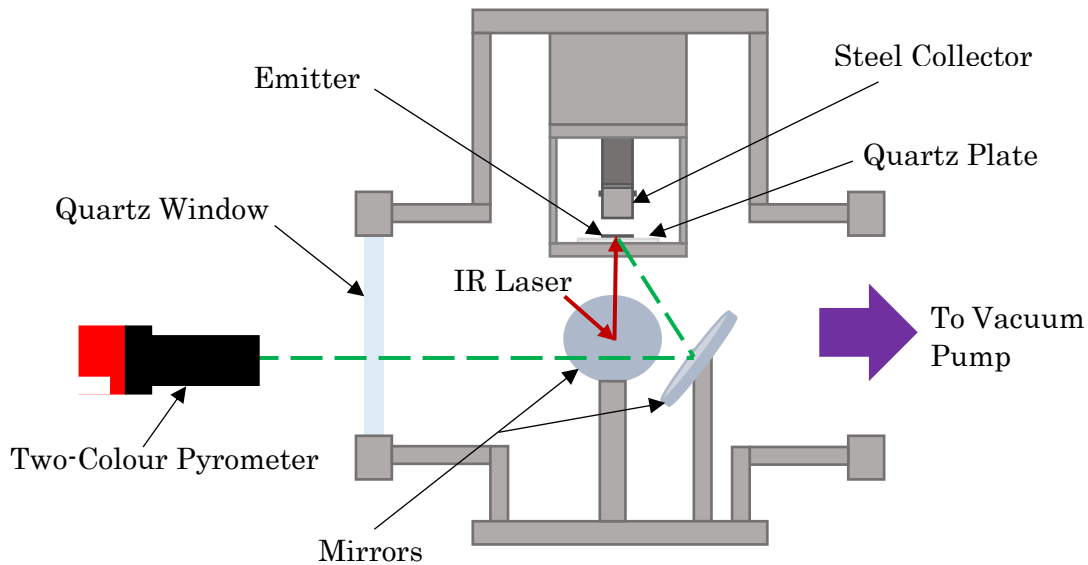


Figure 10. Schematic of the TEC testing rig. Laser enters in the plane of viewing.

For the quantification of thermionic emission, a custom setup was used, as depicted in figure 10. The works of the system was contained in a high vacuum chamber capable of 2.5×10^{-7} Torr, using a turbomolecular pump. On the top of the system was a removable stage containing an insulating quartz platform for the emitter with a hole (7 mm diameter) in the middle and a lowerable steel collector (powered by a piezo-electric motor which was insulated from the collector). Heating was done by a polarised 40 W CO $_2$ laser of wavelength 10.2 – 10.8 μm (Synrad Firestar). For temperature measurement a two-colour optical pyrometer was used (AMETEK Land SPOT R160), it was clamped securely to the rest of the rig. Current was measured using an ammeter accurate to 1×10^{-9} A.

2.3 Methodology

2.3.1 Material Selection and Deposition

Polycrystalline CVD boron doped diamond was selected as the p-type sample for characterisation of the deposited surfaces because it shows almost metal-like conductivity in ambient conditions.⁴⁵ This is important for XPS because it prevents the charging of the sample, leading to better quality spectra. Polycrystalline CVD nitrogen doped diamond was selected as the n-type sample because it has been

shown to be an effective thermionic emitter, it was chosen over phosphorous doped diamond because of availability.⁴⁶

Three metals were chosen of PVD surface coatings for various reasons. Lithium was chosen because it has been shown that both lithium and other alkali metals can form NEA surfaces on doped diamond, along with adsorbing effectively onto oxygen terminated diamond surfaces.^{42,47,48} We wanted to further this research by optimising coating thickness and assess the effect of step annealing. Silver and tin were both chosen because of the similarity of their application as prototype photocathodes in combination with oxygen and lithium.^{49,50} Another reason for alloying silver with lithium is that the conductivity of the alloy is higher than that of pure silver metal.⁵¹

2.3.2 Annealing and Characterisation

For surface characterisation samples *i.e.* boron doped samples, annealing was carried out within the NanoESCA UHV system. All samples were cleaned at 250 °C for 30 minutes in UHV to desorb contaminants before annealing or XPS analysis. Annealing was carried out using a hot filament heater, with the temperature controlled by varying the current passing through the filament. After 30 minutes of annealing the sample was moved to the XPS position in the NanoESCA before XPS scans were taken. XPS was used because it is a core level spectroscopic technique which offers both qualitative and quantitative characterisation of the surface of the sample. It achieves this by measuring the number and kinetic energy of emitted electrons. Scans were taken of all samples after all annealing steps, the regions recorded were a general survey, the carbon 1s orbital region, and the oxygen 1s orbital region, along with these the relevant metal regions were recorded corresponding to the deposited coating.

The annealing temperature steps were either 100 °C or 50 °C depending on the time available and the likelihood of coating desorption, the range of annealing temperature went from 150 °C up to 1000 °C. Once the metal coating was no longer evident on the XPS spectra, characterisation and further annealing was stopped.

After XPS analysis, the thermionic emission ability of the samples was tested, but this time on nitrogen doped samples prepared in the same conditions as the boron doped samples. In doing this analysis after the XPS investigation on the effect of step annealing had been done, a good estimate of the annealing temperature for the formation of a NEA surface was known. Samples were first heated to 300 °C

which was just above the functioning range of the pyrometer, at which point the nitrogen doped diamond became conductive enough to set the emitter/collector separation distance. A distance of 200 μm was used for all samples, also a 25 V bias was applied to the system, with the emitter having the negative bias. For this project, silver/lithium and lithium/oxygen samples and not tin/lithium samples were tested in the thermionic emission rig. For lithium/oxygen samples, the sample was then heated gradually (15 $^{\circ}\text{C}$ per second) up to 500 $^{\circ}\text{C}$ to ensure a clean surface, before being heated to the temperature of NEA presence at the same rate as before, the sample was then kept at the NEA annealing temperature for 5 minutes before the temperature was then cycled between 600 $^{\circ}\text{C}$ and 950 $^{\circ}\text{C}$ to any current. A sample was also run to replicate the conditions of H-terminated nitrogen doped diamond thermionic emission tests, where the sample was simple heated at 10 $^{\circ}\text{C}$ per second from 300 $^{\circ}\text{C}$ to 750 $^{\circ}\text{C}$, for the lithium/oxygen sample the upper temperature was 950 $^{\circ}\text{C}$. Multiple samples were prepared and tested to ensure repeatability of each coating.

3 Results and Discussion

3.1 Hydrogen and Oxygen Terminations

The first samples tested were both hydrogen and oxygen terminated samples without any deposited metal coating. These samples were taken as the controls for the experiments. In order to calibrate the XPS spectrum for a full monolayer coverage, an oxygen terminated single crystal diamond with a thinly grown boron doped diamond CVD film was used. Oxygen termination was done as described in the experimental section. Surface and bulk peak areas for carbon 1s and oxygen 1s were taken from the XPS spectra (see table 2) and showed a carbon to oxygen peak area ratio of 9.8:1 for the bulk measurement and 8.6:1 for the surface measurement, with the analyser positioned at 0° to the sample for the bulk measurement, and 335° for the surface measurement.

Oxygen Terminated Diamond XPS data					
	O 1s raw peak area	C 1s raw peak area	O 1s corrected	C 1s corrected	C:O
Bulk 0°	9735.89	32508.75	2054177	20089948	9.78
Surface 335°	10441.77	30531.80	2203110	18868223	8.56

Table 2. Oxygen terminated diamond XPS peak area data. All figures are in arbitrary units.

In order to directly compare the peak areas, the recorded values had to be divided by the differential photoelectron cross section for the corresponding element. This overcomes the effect that differing cross sectional areas has on peak intensities. For the carbon 1s peak at binding energy 285 eV a differential photoelectron cross section of $0.00161816 \text{ Mbarn}/^\circ$ was used and for oxygen 1s at 532 eV a value of $0.00473956 \text{ Mbarn}/^\circ$ was used.

For the thermionic emission test, a hydrogen terminated nitrogen doped polycrystalline CVD diamond film on a Mo substrate as described in the experimental section was tested, see figure 11. The temperature at which the hydrogen monolayer desorbed from the surface was found to be at around 750°C before which a peak emission of order 1.2 mA was observed. Emission current decreased when the sample temperature stayed at 750°C because with the hydrogen monolayer having desorbed, there was no longer a NEA surface and electron emission was no longer favourable. This was shown to be the case, as when the samples were re-terminated and re-tested, the current returned. When

the peak current and its temperature are put into the Richardson-Dushman equation (1) using the ideal Richardson constant of $1.23 \times 10^6 \text{ A m}^{-2} \text{ K}^{-2}$ a work function of 2.28 eV is calculated for the NEA surface. The ideal Richardson constant was used because there is no known value for λ_R for any of the emitters used in this project. As such, the value of 2.28 eV cannot be considered to be accurate for the reason given before as well as the non-uniformity of a polycrystalline surface and the lack of allowance for the rate of hydrogen desorption. As can be seen from the plot in figure 11, the emission is highly dependent on temperature with very little current below a threshold of 500 °C and a sharp increase in current above that threshold.

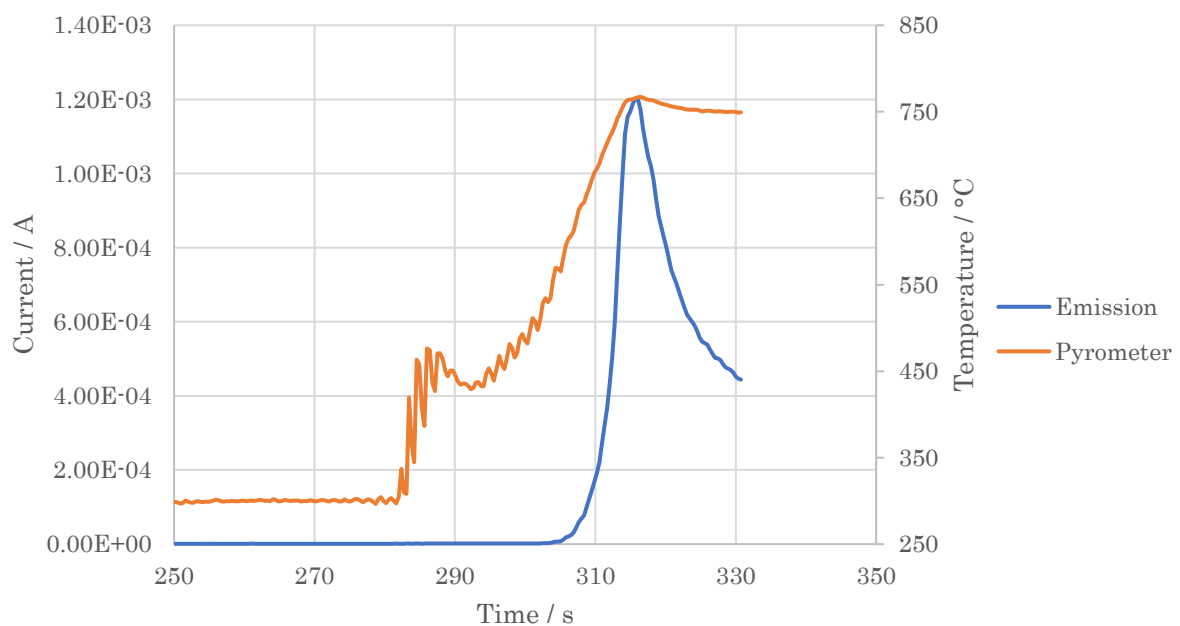


Figure 11. The thermionic emission of hydrogen terminated, nitrogen doped CVD diamond.

Due to oxygen terminated diamond have a positive electron affinity, thermionic emission tests of oxygen terminated diamond were not carried out.

3.2 Silver/Lithium

The first coatings tried were those of a silver lithium alloy. These were deposited onto both hydrogen terminated and oxygen terminated, boron doped diamond. The effectiveness of the deposition was investigated using XPS. It was with the silver lithium alloy coatings that the effect of both termination and percentage surface coverage was investigated. The stability of the coating after heating to emissive

temperatures was also investigated. The first set of samples prepared had a deposition of silver and lithium as described in the experimental section that covered 25% of the surface area. The deposition process was only found to be effective when the diamond surface was oxygen terminated beforehand. This is due to the affinity that lithium has to oxygen given by its electropositivity. Despite being boron doped diamond samples, these were tested for thermionic emission. No significant emission was observed. Further tests on samples with increasing silver lithium coverage also showed no observable thermionic emission. The final samples tested with 100% metal coating coverage were the ones used for XPS analysis for ease of focusing the analyser onto the coatings.

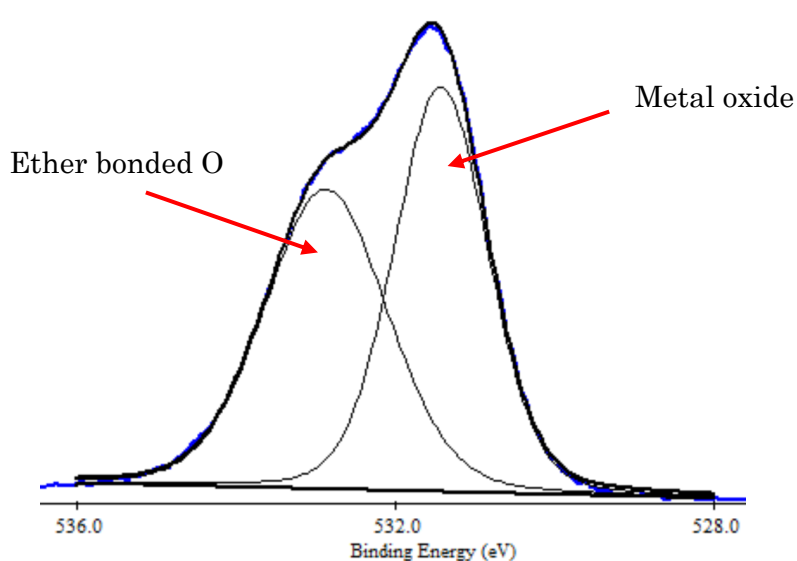


Figure 12. Oxygen 1s XPS spectrum for silver/lithium coated BDD sample. The blue line indicates the recorded spectrum, the emboldened black line is the optimised spectrum with baseline, the thin black lines are the component peaks. The y-axis is counts in arbitrary units.

Despite the lack of a NEA surface, there was some interesting surface chemistry observed. The oxygen peak showed two environments at binding energies of 531.4 eV and 532.9 eV, see figure 12. The peak at 532.9 eV matches closely with the value for ether bonded oxygen which is 532.8 eV.⁵² The peak at the lower binding energy of 531.4 eV is likely to be from metal oxide, especially Li_2O above the initial oxygen termination monolayer. There is some uncertainty in the bonding regime of the oxygen monolayer as a ketone bonded oxygen would appear at 532.2 eV as such is almost indistinguishable from the ether form. The peak area ratio for the two environments was almost exactly 1:1 (see table 2).

XPS Peak Area Ratios for Ag/Li coated samples

Peak	O 1s 531.4	O1s 532.9	Ag 3d	C 1s	Li 1s 51.4	Li 55.8	Σ Li 1s
$\times \Sigma$ O 1s	0.51	0.49	0.11	4.98	7.18	24.44	31.62

Table 2. Ratios of all corrected peak areas to the total oxygen 1s peak area. Binding energies in eV.

The peak for silver 3d showed that the only environment present was that of metallic silver with the 3d_{5/2} peak at 368.3 eV and 3d_{3/2} at 374.3 eV.⁵⁴ Therefore the silver did not form an oxide either during deposition or after exposure to air. The occurrence of alloying is however possible as an alloyed metallic silver peak occurs at identical binding energies to pure metallic silver. The lithium peak is also curious in that it gave two peaks, see figure 13. The peak with the larger area at a binding energy of 55.8 eV is indicative of Li₂O with the peak at 51.4 eV is likely to be that of lithium metal, although the binding energy is unusually low, this could be due to alloying with the silver deposited above it.⁵³ As with all lithium XPS, there is a degree of uncertainty in terms of peak intensity and area introduced by lithium having a very small cross section, for this there are rectifying factors but in truth there is still inaccuracy as far as they are concerned.

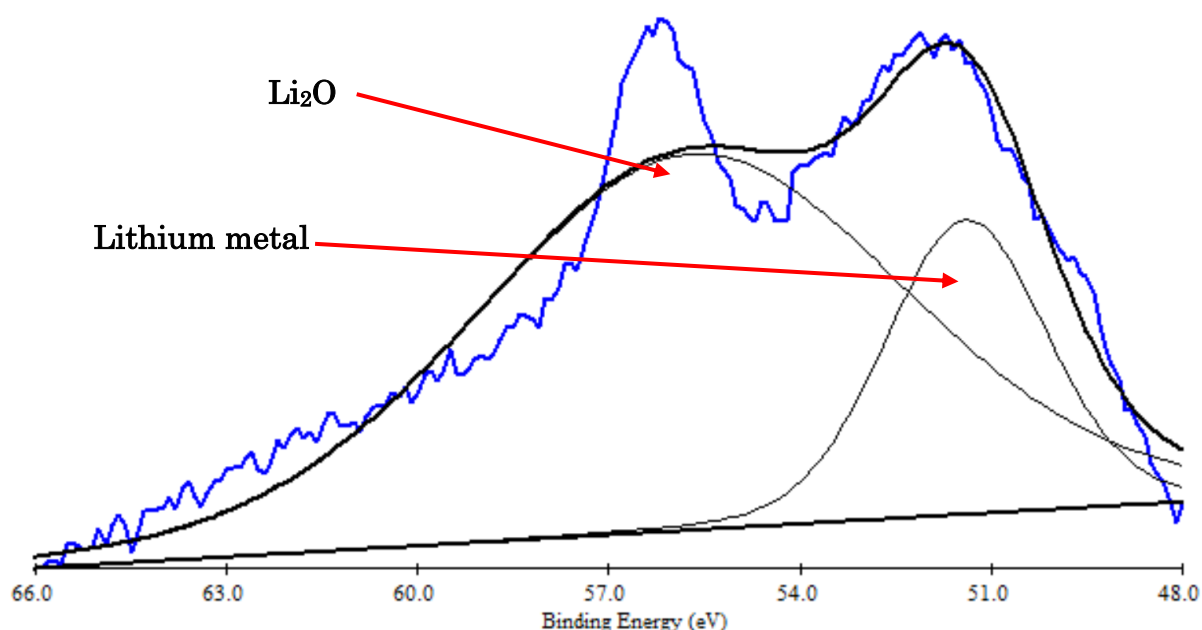


Figure 13. Lithium 1s XPS spectrum for silver/lithium coated BDD sample. The blue line indicates the recorded spectrum, the emboldened black line is the optimised spectrum with baseline, the thin black lines are the component peaks. The y-axis is counts in arbitrary units.

Overall, the use of a silver lithium alloy as a NEA surface was found to be ineffective so other coatings were investigated. Although, the thermionic emission of nitrogen doped diamond samples with a silver lithium alloy coating was not tested, this may explain the poor results as boron doped diamond samples tend not to emit very well thermionically whatever the termination or coating due to its high work function.

3.3 Lithium/Oxygen

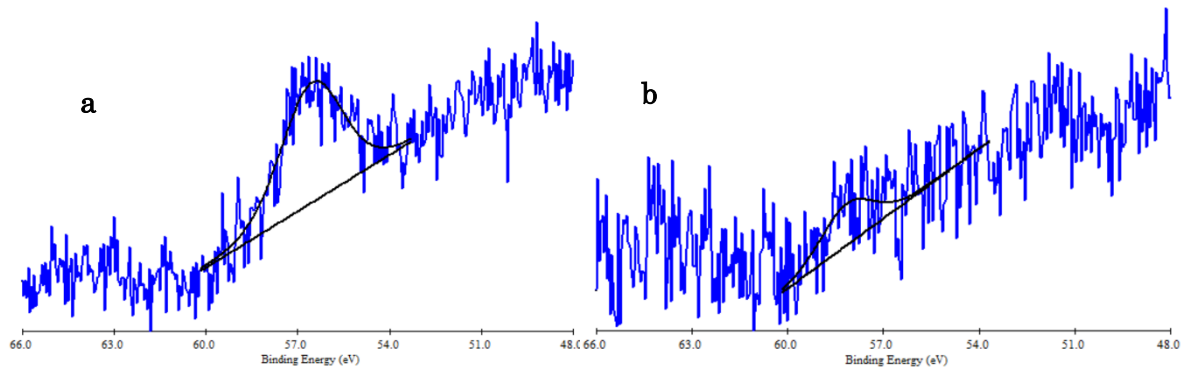


Figure 14. XPS spectra of the Li 1s region after annealing for 30 min. to a) 900 °C and b) 970 °C. The blue line indicates the recorded spectrum, the emboldened black line is the optimised spectrum with baseline. The y-axis is counts in arbitrary units.

A lithium oxygen coating was most likely to form a NEA surface given the success of prior research, in this case, the effect of step annealing was investigated. The initial characterisation by XPS showed that lithium was present in bulk quantities after deposition from ambient temperature up to a annealing temperature of 800 °C at which point the coating was less than a monolayer and a NEA surface was apparent, see figure 15. This degree of coating was stable to over 900 °C, but any trace of remaining lithium desorbed when the sample reached temperatures above 950 °C, see figure 14. At all temperatures only one lithium environment was apparent, that of Li^+ , although the binding energy was shifted up by *ca.* 1 eV in all cases, which may have been due to band bending or shifting of the Fermi level at the surface.

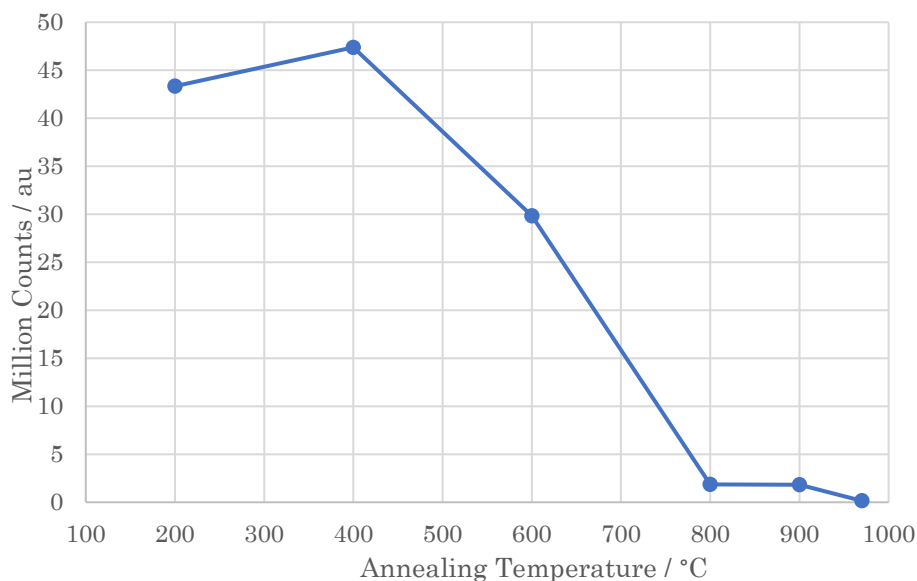


Figure 15. The corrected XPS peak areas of Li 1s at binding energy 56.5 eV after step annealing.

For the carbon 1s region of the XPS spectra taken the dominant form of carbon present after annealing at lower temperatures is the carbonate form at a binding energy of 291.4 eV, with the pure carbon peak at 285.5 eV being less intense, see figure 16. The source of the carbonate peak is most likely to be from the reaction of Li_2O with atmospheric CO_2 to form lithium carbonate. After annealing to 600 °C there was no longer a carbonate response on the spectra.

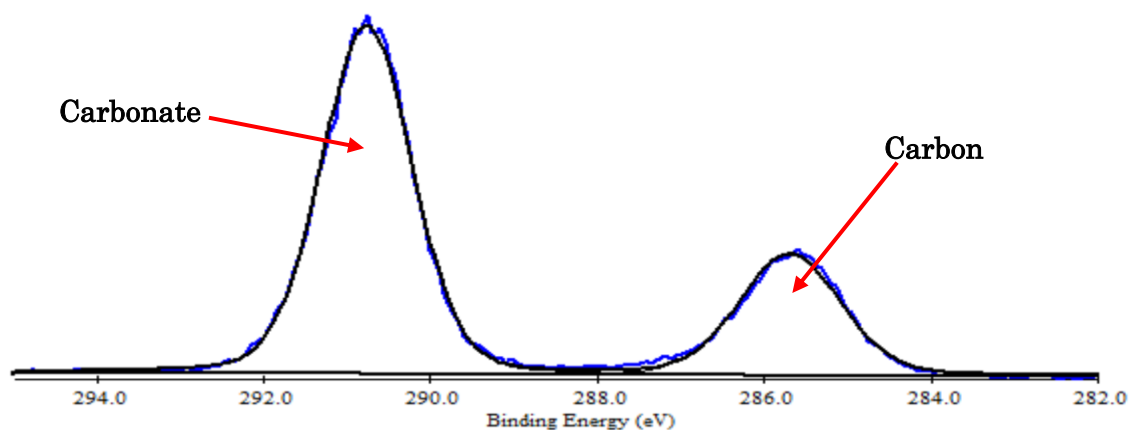


Figure 16. XPS spectrum of the C 1s region after annealing for 30 min. to 200 °C. The blue line indicates the recorded spectrum, the emboldened black line is the optimised spectrum with baseline. The y-axis is counts in arbitrary units.

The oxygen 1s region after annealing at lower temperatures gave a signal in the carbonate region at binding energy 532.7 eV, confirming the carbon 1s responses. After annealing to 600 °C, just as the carbonate peak disappeared for the carbon 1s spectra, the oxygen 1s peak changed to a similar form to the oxygen peak for the silver lithium coated sample (figure 12). From this it was apparent that the initial deposition of lithium onto an oxygen monolayer was consistent between the two sample sets, although the response was again shifted by 1 eV.

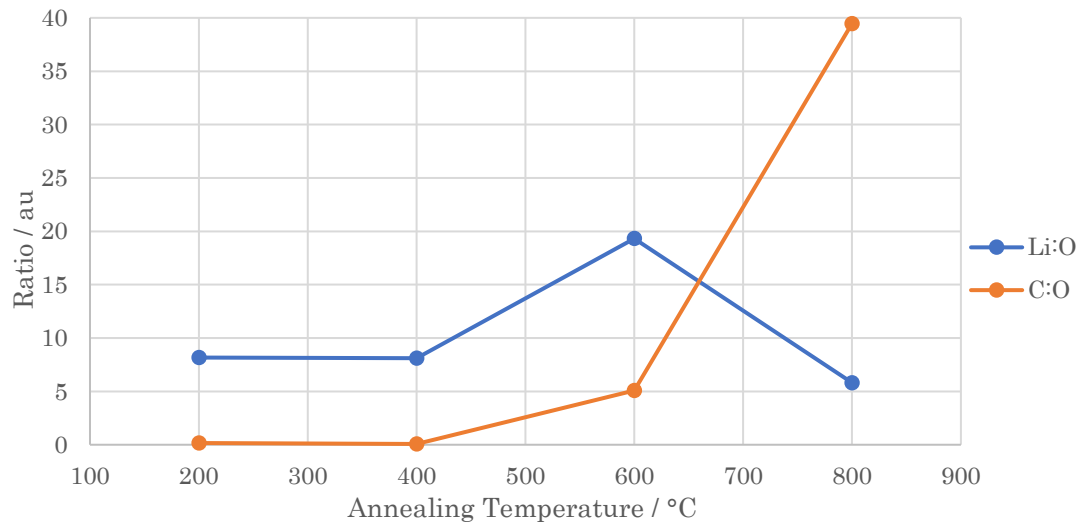


Figure 17. Ratios of corrected XPS peak areas to the total oxygen 1s peak area after step annealing.

After the annealing to 600 °C the carbon to oxygen ratio was at 5:1 implying that a full monolayer as determined before would occur after annealing to a temperature between 600 and 700 °C, with the ratio for a full monolayer being *ca.* 10:1. After annealing to 800 °C, the oxygen 1s response was very weak and when the peak area ratio of carbon to oxygen is compared to the purely oxygen terminated sample, oxygen is at much less than a full monolayer with a ratio of almost 40:1 carbon:oxygen, see figure 17.

The nitrogen doped diamond samples which had been coated in the same conditions as the boron doped samples were tested for thermionic emission as explained in the experimental section. It was found that the lithium oxygen coating was able to produce a NEA surface and produce thermionic emission in a similar vein to the hydrogen terminated samples, see figure 18. However, when compared to the hydrogen terminated samples, the emission current was considerably weaker, with a peak current of just under 9 μ A, over two orders of magnitude weaker than that of the hydrogen terminated samples. In terms of heat stability, the lithium oxygen coatings were more thermally stable than a hydrogen monolayer since they were able to be heated to temperatures above those at which

a hydrogen monolayer would desorb (750 °C). However, significant emission from lithium oxygen coated samples only occurred at temperatures of 800 °C and above, at which point significant surface desorption occurred. This did however confirm that the NEA surface would be achieved after heating to 800 °C, at which point a less than full lithium oxygen monolayer had been observed. The work function for the sample at the point of the highest current was calculated to be 3.27 eV, almost exactly 1 eV higher than the value calculated for the hydrogen. The value of 3.27 eV is entirely consistent with literature figures for the work function of NEA surfaces on highly nitrogen doped diamond samples.^{40,54}

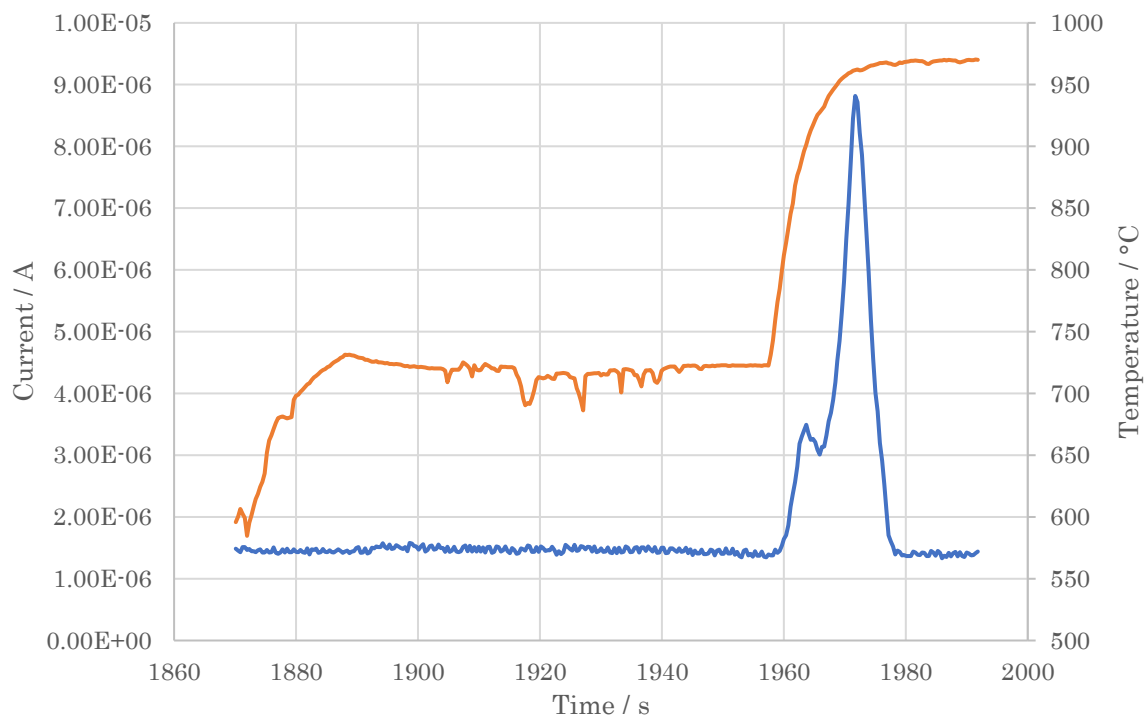


Figure 18. The thermionic emission of lithium oxygen coated, nitrogen doped diamond.

3.4 Tin/Lithium

Towards the end of the project, tin lithium coatings were investigated, although time constraints limited the amount of data that could be acquired. The XPS analysis on the boron doped samples displayed the great deal of surface chemistry that occurs with metal alloys and oxides during the step annealing process under vacuum.

The tin 3d region has different binding energies depending on the oxidation state, two of these were apparent in the spectra taken due to metallic tin and its dioxide Sn(IV)O₂ (stannic oxide), the monoxide Sn(II)O (stannous oxide) was not clearly

observed. Metallic tin gives a $3d_{5/2}$ binding energy of 485.0 eV with spin-orbit splitting $\Delta = 8.41$ eV for the $3d_{3/2}$ peak, whereas Sn(IV) gives a $3d_{5/2}$ binding energy of 486.8 eV with the same spin-orbit splitting, see figure 19.^{53,54} A Sn(II) $3d_{5/2}$ binding energy would be at 485.9 eV, bisecting the $3d_{5/2}$ binding energies for metallic tin and Sn(IV).⁵⁵

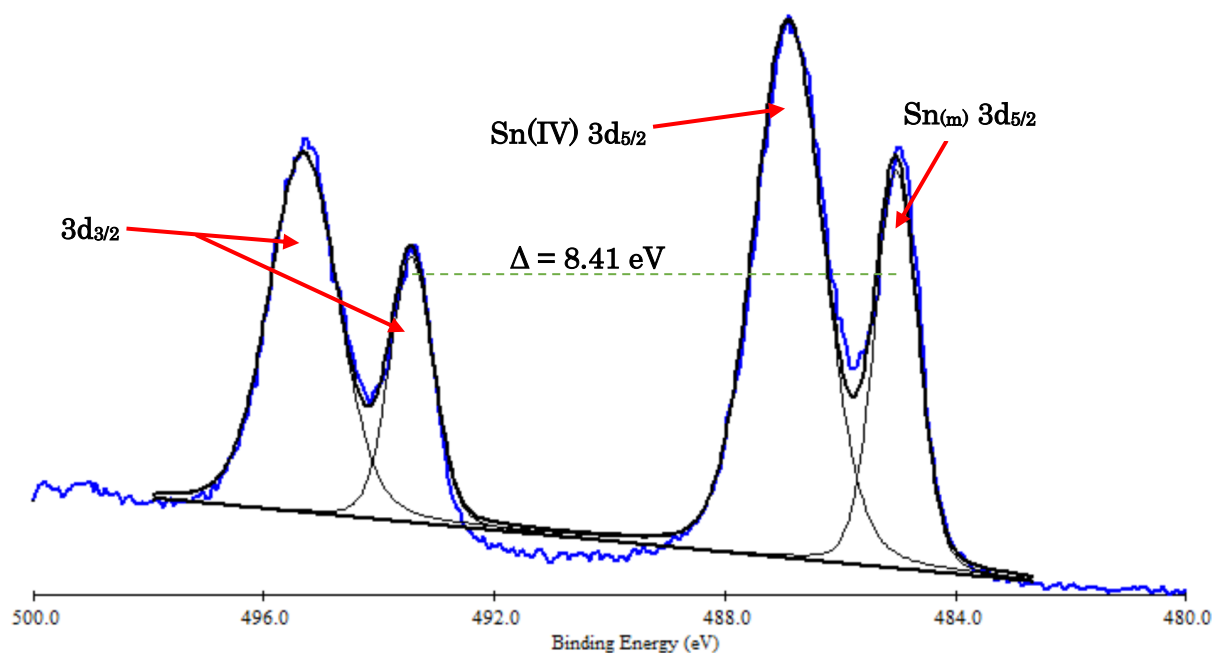


Figure 19. XPS spectrum of the Sn 3d region after annealing for 30 min. to 450 °C. The blue line indicates the recorded spectrum, the emboldened black line is the optimised spectrum with baseline, the thin black lines are the component peaks, the green dashed line indicates spin-orbit splitting of the Sn 3d responses. The y-axis is counts in arbitrary units.

At lower temperatures the Sn(IV) peak was dominant, with very little intensity from the metallic peak, see figure 20. This is due to the upper layers (further from the diamond surface) of the tin deposition having reacted with oxygen in the deposition chamber to form stannic oxide, it also confirms that the thickness of the tin deposition was over the limit of XPS analysis surface penetration of *ca.* 10 nm. The reaction most likely happened in the deposition chamber at high temperature as tin does not readily react with room temperature oxygen. Stannous oxide is thermodynamically less stable than stannic and conditions in the deposition chamber were not correct for its formation. After annealing to 450 °C for 30 minutes the elemental tin peak became much more intense, as did the Sn(IV) peak. From this temperature of annealing upwards the elemental tin intensity remained stable, however the Sn(IV) peak intensity decreased rapidly. The rate at which the Sn(IV) peak intensity diminished can be compared to the rate at which the oxygen

1s peak relating to the O²⁻ ion diminished. After annealing to 750 °C a significant amount of both Sn(IV) and Sn metal was still present on the diamond sample.

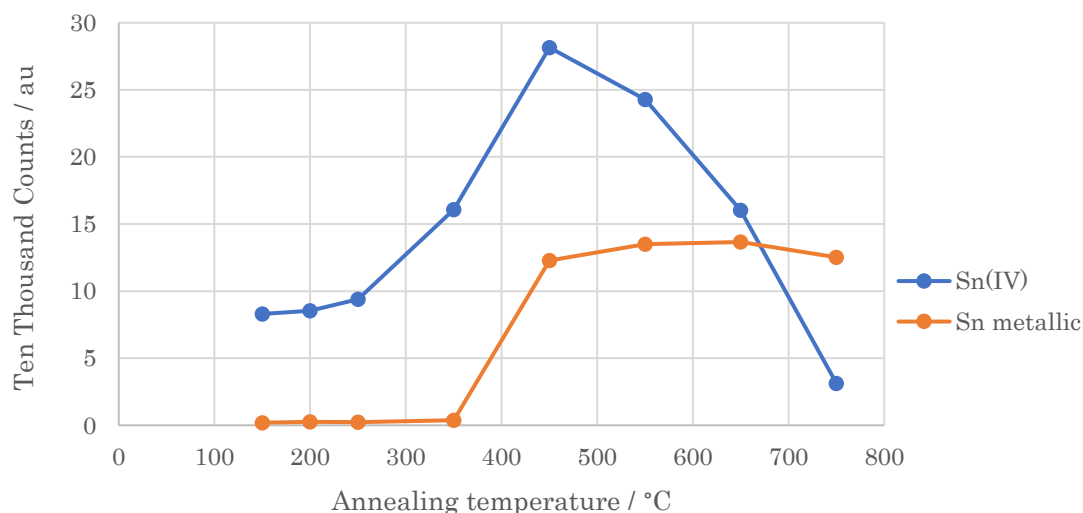


Figure 20. Corrected XPS peak areas of tin metal and tin(IV) after step annealing.

The oxygen 1s region had two major peaks, one at a binding energy of 530.6 eV and one at 532.8 eV. The peak at 530.6 eV is that for a metal oxide in this case the O²⁻ ion of both Li₂O and Sn(IV)O₂. The peak at 532.8 eV is for ether bonded oxygen, found as the surface termination for the diamond sample. As seen with the Sn(IV) peak, the O²⁻ peak intensity reduces significantly as Sn(IV)O₂ desorbs from the surface. The sharper decline of the O²⁻ peak intensity compared to the Sn(IV) intensity can be explained by the desorption of Li₂O at the same time.

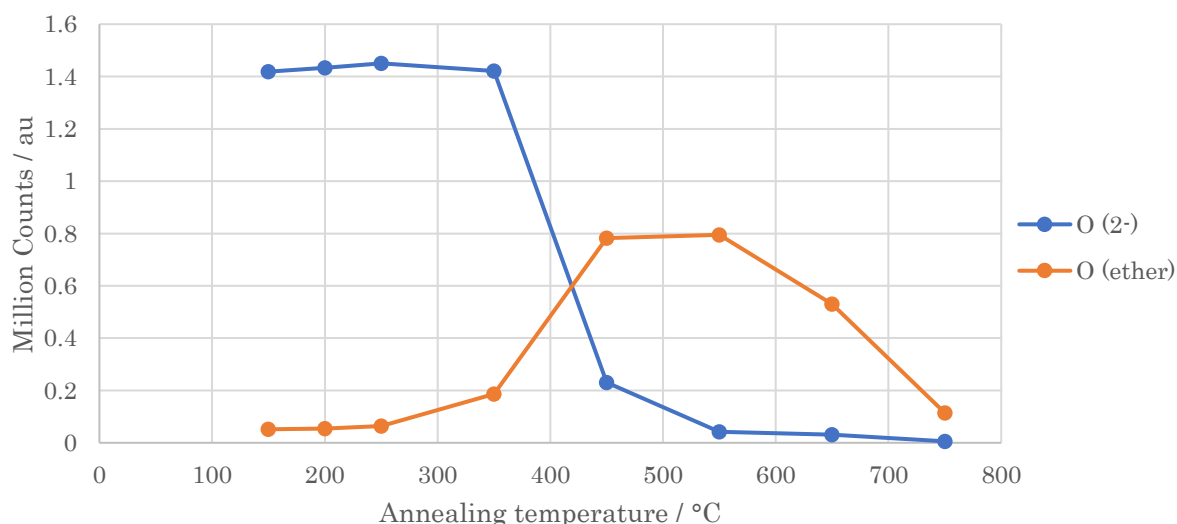


Figure 21. Corrected XPS peak areas of O²⁻ (530.6 eV) and O ether (532.8 eV) after step annealing.

The stability of the ether bonded oxygen peak is comparable to that of the lithium oxygen samples previously discussed, see figure 22. The carbon to oxygen (ether) peak area ratio is very similar in both cases after annealing to temperatures of 450 °C and higher, with less than monolayer values of *ca.* 39:1 at both 750 °C for the tin lithium sample and 800 °C for the lithium oxygen sample. From the pure oxygen termination data a full monolayer would have a ratio of 9.78:1 although this figure does not distinguish between ether and ketone bonded oxygen. As such, the figure of *ca.* 5:1 at 600 – 650 °C would represent two monolayers of oxygen at the diamond surface, the upper of which would be as lithium oxide.

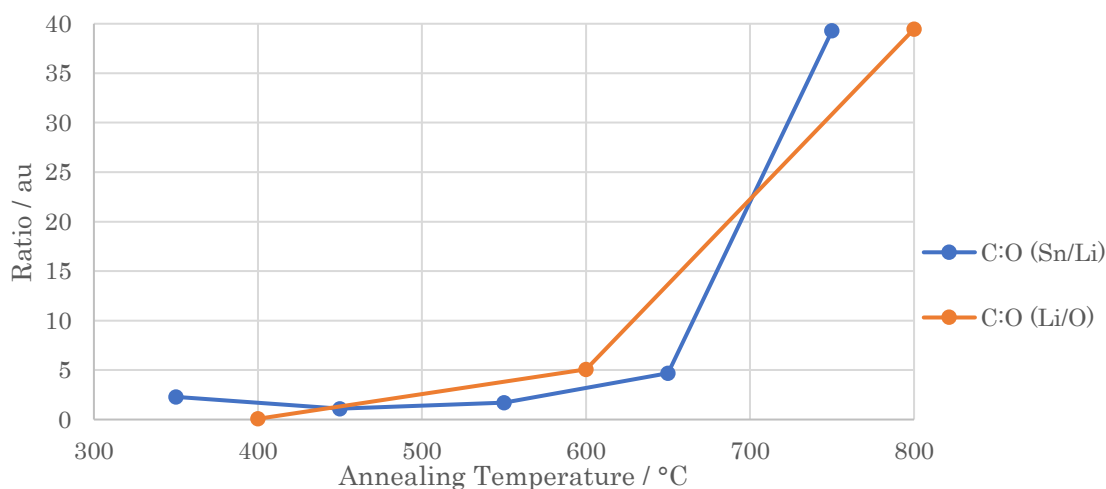


Figure 22. Ratios of corrected XPS peak areas for carbon 1s to the oxygen (ether) 1s for both the lithium oxygen coating and tin lithium coating after step annealing.

The lithium region in the XPS spectra for the tin lithium coated sample was again similar to that of the lithium oxygen coated samples in some respects, see figure 23. The binding energy was almost identical at 56.5 eV, indicating that only a Li^+ bonding regime was present, without any elemental metallic lithium. Therefore, it seems unlikely that much if any alloying between the lithium and tin occurred. In terms of stability after annealing, the lithium peak was similar to the stability of the O^{2-} ion in the sample, the intensity of the peak appeared to diminish after annealing to 350 °C, although it did not diminish as rapidly as the O^{2-} peak due to O^{2-} being bonded in two different environments. Quantitatively for the tin lithium sample, the lithium peak intensity was a quarter of the intensity of the lithium oxygen sample at most steps of the annealing sequence, indicating similar chemistry in both samples, independent of the presence of tin. After annealing to 750 °C, however, the lithium peak intensity was almost nil, indicating that very little lithium remained on the sample. If a NEA surface was apparent after

annealing to 650 °C, it is unlikely to be present on these samples after annealing to 750 °C.

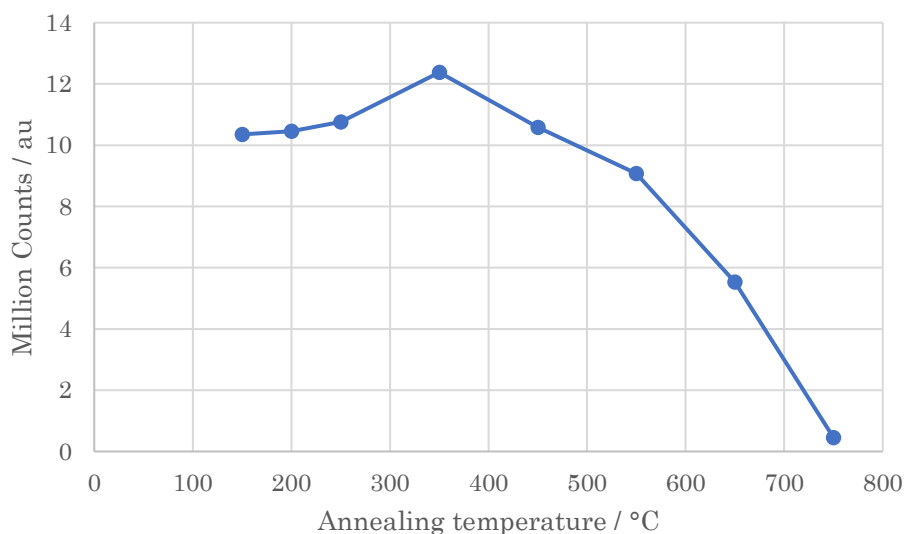


Figure 23. The corrected XPS peak areas of Li 1s at binding energy 56.5 eV after step annealing.

As for the lithium oxygen coating, a carbonate peak due to Li_2CO_3 was present in the carbon region of the XPS spectra taken. The carbonate peak had desorbed in entirety after annealing to 450 °C.

With these comparisons, it is possible that after annealing to 650 °C a NEA surface begins to form. Due to time constraints, it was not possible to anneal the sample to higher temperatures or to test nitrogen doped samples in the thermionic kit to test this. Although the effectiveness of tin metal as a NEA surface is still unknown.

3.5 Caveats

The foremost caveat in these data is the difficulty that the XPS technique has in detecting atoms with small cross-sectional radii, of which lithium is one. This doesn't pose much of a problem for the qualitative aspect of XPS spectra, but it does lead to a certain amount of uncertainty with regard to the quantitative nature of the spectra, for example the lithium peak for the tin lithium coated samples after annealing to 750 °C was weak in its intensity (see figure 24), yet with the factor applied the integrated peak area was almost half a million counts, which was 10 times that of oxygen, stoichiometrically this is unlikely. The correctional cross-section factors for each atom's spectra does help in this matter, but there is still a degree of uncertainty when comparing integrated peak areas of

different atoms when some are as sensitive to XPS as tin and others are as insensitive as lithium.

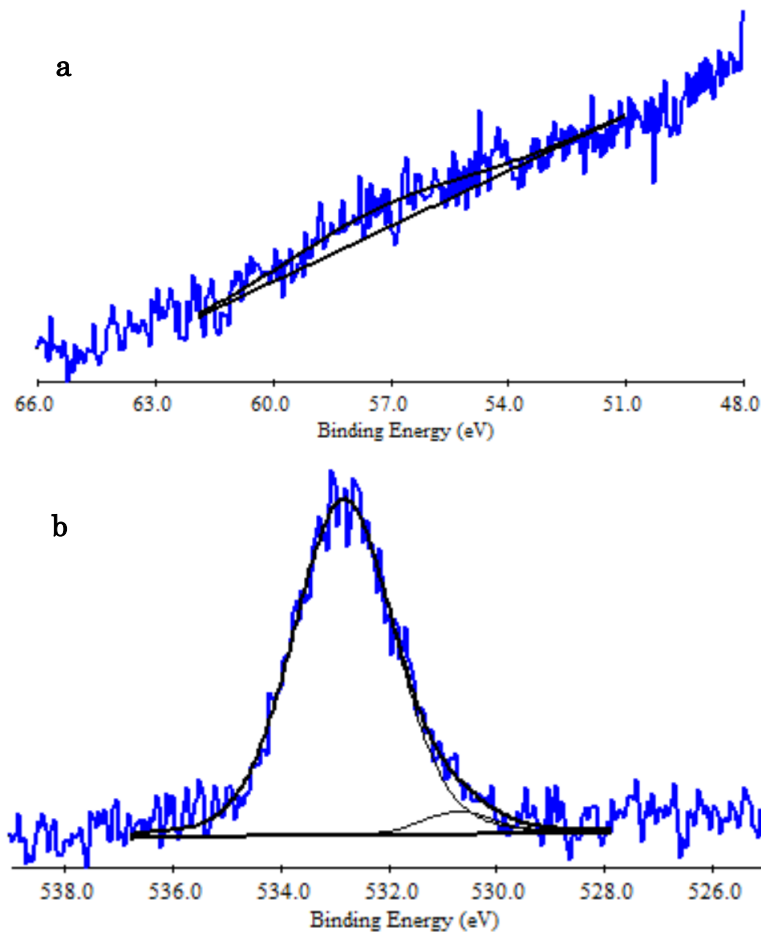


Figure 24. XPS spectra of Sn/Li coated sample after annealing for 30 min. to 750 °C, a) Li 1s b) O 1s. . The blue line indicates the recorded spectrum, the emboldened black line is the optimised spectrum with baseline, the thin black lines are the component peaks. The y-axis is counts in arbitrary units.

The measurement of temperature for annealing in the UHV NanoESCA facility when done by comparing the current flowing through the filament heater to a chart estimating the temperature that the filament would reach. With diamond being such a good thermal conductor this was less of a problem, but the accuracy of the reading may have been rather poor with a large amount (± 20 °C) of error likely. The use of a pyrometer aimed at the sample in the NanoESCA would have helped with the consistency of temperature measurements between the XPS system and the thermionic emission testing system.

4 Conclusions

4.1 Summary

Three metal oxygen coatings for p-type and n-type doped polycrystalline CVD diamond were analysed for their ability to form a negative electron affinity surface to enhance the diamond's ability for thermionic emission by effectively lowering the emitter's work function. The effect of different terminations, different proportions of coating coverage, and step annealing was also tested.

For silver lithium coatings, it was found that a stable coating was only achieved when the diamond sample was terminated with oxygen; hydrogen terminated samples were not stable at emitting temperatures. Metallic lithium was found to alloy with the silver metal as well as form Li_2O . The coating was found to not form a NEA surface and the boron doped diamond sample underneath was not capable of thermionic emission at the temperatures tested. The proportion of coating coverage made little effect on the ability of the sample to emit thermionically.

Lithium oxygen coatings are already known for their ability to form a NEA surface and this was shown to be the case with a work function of 3.27 eV found for lithium oxygen coated nitrogen doped diamond samples after heating to 800 °C. With step annealing, bulk lithium oxide was present until annealing at a temperature of 800 °C for 30 minutes, after which a less than monolayer coverage of lithium atoms remained. The lithium coating desorbed fully after annealing to 970 °C.

Tin lithium coatings were characterised but not tested for thermionic emission due to time constraints. It was found that tin was present in both stannic oxide (Sn^{+4}) and metallic forms, stannic oxide formed the top layer of the coating and desorbed gradually after annealing to 550 °C and upwards. Metallic tin was stable on the sample at all the tested annealing temperature (highest 750 °C). Lithium was found only in its ionic Li^+ form, and desorbed in a similar regime to Sn^{+4} . Oxygen was found to be in both metallic oxide form and ether bonded form, indicating that the termination monolayer on the diamond was largely of ether bonded oxygen rather than ketone. If a NEA surface formed, it is most likely to have formed after annealing to 650 °C, and absent after annealing to 750 °C.

4.2 Future Work

To confirm the inability of the silver lithium coating to form a NEA surface, annealing to higher temperatures as well as testing the coating on nitrogen doped diamond samples in the thermionic emission kit would be key data to obtain. Perhaps reduced the proportion of silver compared to lithium would also improve the chances of the coating forming a NEA surface.

For the lithium oxygen coated sample, being able to step anneal a nitrogen doped sample and then take thermionic emission measurements after each step within the NanoESCA would give better data for analysis, unfortunately this operation was not possible during this project but would be possible now that the instruments are now fully operational.

A great deal more data could be taken for the tin lithium samples, foremost would be thermionic emission testing of nitrogen doped samples after step annealing. Also, XPS spectra can be taken of boron doped samples after annealing to even higher temperatures to observe the stability and thickness of the coating.

The variation of thickness of the coating over the diamond surface would be interesting data to analyse, especially after annealing to temperatures at which the coating appears to be less than a full monolayer. This could be achieved with X-ray photoemission electron microscopy, or by doing XPS while rastering the aim of the probe in small amounts, this would be done in the NanoESCA system by moving the sample along the x-axis of the system. This would allow measurement at 1 mm intervals along one axis.

Phosphorous doped n-type diamond is known to be a superior thermionic emitter to nitrogen doped diamond, with a recorded effective work function of 0.9 eV for hydrogen terminated samples with a phosphorous dopant concentration of *ca.* 5×10^{18} atoms cm^{-3} .⁵⁶ The stability of metal oxygen coatings at high temperature and their effect on the work function would be interesting to investigate.

Beta radiation has been shown to enhance thermionic emission from nitrogen doped diamond samples. Using a ^{63}Ni collector can reduce the threshold emission temperature by 58 ± 11 °C and also cause a 2.7-fold increase in current density compared to an equivalent ^{59}Ni collector.⁵⁷ In this case the beta radiation source was located in the collector, a more effective way of doing this would be to have the beta source in the emitter. This has been proposed to be done by growing the

diamond with ^{14}C included lattice structure, another method would be to give the diamond a coating incorporating a beta emitting metal like ^{90}Sr or ^{63}Ni , or perhaps simply terminating the diamond with a tritium/hydrogen mixture.

In terms of other metal coatings, several candidate materials present themselves. For similar reasons to why silver and tin were chosen, gallium and antimony, which are both used in photocathode emitters, could be used as coating with alkali metals like caesium or lithium. Metal combinations like these tend to have low work functions and could very well form NEA surfaces on doped diamond samples for thermionic emission. Titanium and tungsten are other metals with properties that could lead it to form a NEA surface on diamond. Titanium is commonly used to form Schottky junctions with diamond and is highly thermally stable.⁵⁸ It forms a carbide at the interface with diamond as such, an oxygen termination would not be necessary for stability. The carbide on its own has a work function of 3.8 eV at room temperature, in a thin layer this could result in very efficient thermionic emission.⁵⁹ Tungsten forms a similar carbide at the diamond surface.⁶⁰ Caesiated titanium has been used as an emitter for photon-enhanced thermionic emission and shown to have a work function that can reach almost 1 eV, a similarly caesiated tungsten emitter's work function is also low at *ca.* 1.7 eV.¹¹ If a thin lithiated titanium or caesiated titanium coating could be deposited onto a n-type doped diamond film and then annealed under vacuum a NEA surface may form.

5 Bibliography

1. T. L. Martin, K. M. O'Donnell, H. Shiozawa, C. E. Giusca, N. A. Fox, S. R. P. Silva, D. Cherns, *Materials Research Society Symposia Proceedings*, 2011, **1282**, 169.
2. E. Becquerel, *Annales de Chimie et de Physique*, 1853, **39**, 48.
3. P. A. Redhead, *Journal of Vacuum Science & Technology A*, 1998, **16**, 1394.
4. O. W. Richardson, *Philosophical of the Cambridge Philosophical Society*, 1901, **11**, 286.
5. C. R. Crowell, *Solid State Electronics*, 1965, **8**, 395.
6. T. D. Musho, W. F. Paxton, J. L. Davidson, D. G. Walker, *Journal of Vacuum Science & Technology B*, 2013, **31**, 021401-1.
7. M. E. Kiziroglou, X. Li, A. A. Zhukov, P. A. J. de Groot, C. H. de Groot, *Solid-State Electronics*, 2008, **52**, 1032.
8. G. Smestad, *Solar Energy Materials & Solar Cells*, 2004, **82**, 227.
9. M. N. Lakhoua, *International Journal of Physical Sciences*, **7**, 2012, 5493.
10. G. L. Bennett, *Proceedings of the 24th Intersociety Energy Conversion Engineering Conference*, 1989.
11. V. Vershchetin, E. Vasilevskaya, and E. Kamenetskaya, *Outer Space: Politics and Law*, Progress Publishers, Moscow, 1987.
12. J. W. Schwede, I. Bargatin, D. C. Riley, B. E. Hardin, S. J. Rosenthal, Y. Sun, F. Schmitt, P. Pianetta, R. T. Howe, Z.-X. Shen, N. A. Melosh, *Nature Materials*, 2010, **9**, 762.
13. M. A. Green, K. Emery, Y. Hishikawa, W. Warta, *Progress in Photovoltaics*, 2010, **19**, 84.
14. K. A. A. Khalid, T. J. Leong, K. Mohamed, *IEEE Transactions on Electron Devices*, 2016, **63**, 2231.
15. G. N. Hatsopoulos, E. P. Gyftopoulos, *Thermionic Energy Conversion: Processes and Devices*, MIT Press, Cambridge MA, 1973.
16. F. Morini, E. Dubois, J. F. Robillard, S. Monfray, T. Skotnicki, *Physica Status Solidi A*, 2014, **211**, 1334.
17. T. L. Westover, A. D. Franklin, B. A. Cola, T. S. Fisher, R. G. Reifenberger, *Journal of Vacuum Science & Technology B*, 2010, **28**, 423.
18. S. Basu, Z. Zhang, C. Fu, *International Journal of Energy Research*, 2009, **33**, 1203.

19. J. Lee, I. Bargatin, N. Melosh, R. Howe, *Applied Physics Letters*, 2012, **100**, 173904.
20. M. Werner, R. Locher, *Reports on Progress in Physics*, 1998, **61**, 1665.
21. M. H. Grimsditch, A. K. Ramdas, *Physical Review B*, 1975, **11**, 3139.
22. J. E. Graebner, S. Jin, G. W. Kammlott, J. A. Herb, C. F. Gardinier, *Applied Physics Letters*, 1992, **60**, 1576.
23. B. Dischler, C. Wild, *Low-Pressure Synthetic Diamond: Manufacturing and Applications*, Springer-Verlag, Berlin, 1998.
24. J. B. Hannay, *Proceedings of the Royal Society of London*, 1880, **30**, 188.
25. H. Moissan, *Comptes Rendus de l'Académie des Sciences, Paris*, 1894, **118**, 320.
26. N. V. Sidgwick, *The Chemical Elements and their Compounds*, 1950, Oxford University Press, London.
27. F. P. Bundy, H. T. Hall, H. M. Strong, R. H. Wentorf, *Nature*, 1955, **176**, 51.
28. S. Matsumoto, Y. Sato, M. Kamo, N. Setaka, *Japanese Journal of Applied Physics*, 1982, **21**, L183.
29. M. Kamo, Y. Sato, S. Matsumoto, N. Setaka, *Journal of Crystal Growth*, 1983, **62**, 642.
30. P. W. May, *Philosophical Transactions of the Royal Society A*, 2000, **358**, 473.
31. W. Saslow, T. K. Bergstresser, M. L. Cohen, *Physical Review Letters*, 1966, **16**, 354.
32. R. S. Sussmann, *CVD Diamond for Electronic Devices and Sensors*, Wiley, Chichester U.K., 2009.
33. L. Pauling, *The nature of the chemical bond and the structure of molecules and crystals*, Cornell University Press, Ithaca NY, 1960, 3rd ed..
34. B. Cordero, V. Gómez, A. E. Platero-Prats, M. Revés, J. Echeverría, E. Cremades, F. Barragán, S. Alvarez, *Dalton Transactions*, 2008, **21**, 2832.
35. A. Rowan, MSci Thesis, University of Bristol, 2017.
36. C. F. Chen, S. H. Chen, *Diamond and Related Materials*, 1995, **4**, 451.
37. A. Cheesman, PhD Thesis, University of Bristol, 2006.
38. S. Skokov, B. Weiner, M. Frenklach, *Physical Review B*, 1994, **49**, 11 374.
39. X. M. Zheng, P. V. Smith, *Surface Science*, 1992, **262**, 219.
40. L. Diederich, O. M Küttel, P. Aebi, L. Schlapbach, *Surface Science*, 1998, **418**, 219.
41. F. Maier, J. Ristein, L. Ley, *Physical Review B*, 2001, **64**, 165411-1.

42. M. J. Rutter, J. Robertson, *Physical Review B*, 1998, **57**, 9241.
43. W. G. Spitzer, C. A. Mead, *Physical Review*, 1964, **134**, A713.
44. S. Núñez-Sánchez, H. Andrade, C. Harwood, I. Bickerton, N. A. Fox, M. Cryan, *The 6th International Conference on Metamaterials, Photonic Crystals and Plasmonics*, 2015.
45. P. Ashcheulov, J. Šebera, A. Kovalenko, V. Petrák, F. Fendrych, M. Nesládek, A. Taylor, Z. Vlčková, O. Frank, L. Kavan, M. Dračinský, P. Hubík, J. Vacík, I. Kraus, I. Kratochvílová, *European Physical Journal B*, 2013, **86**, 443.
46. F. A. M. Koeck, R. J. Nemanich, Y. Balasubramaniam, K. Haenen, J. Sharp, *Diamond & Related Materials*, 2011, **20**, 1229.
47. S. Petrick, C. Benndorf, *Diamond & Related Materials*, 2001, **10**, 519.
48. M. W. Geiss, J. C. Twichell, *Applied Physics Letters*, 1995, **67**, 1328.
49. K. S. Neil, C. H. B. Mee, *Physica Status Solidi A*, 1970, **2**, 43.
50. J. Azevedo, S. D. Tilley, M. Schreier, M. Stefik, C. Sousa, J. P. Araújo, A. Mendes, M. Grätzel, M. T. Mayer, *Nano Energy*, 2016, **24**, 10.
51. J. A. Rodriguez, J. Hrbek, *Journal of Physical Chemistry*, 1994, **98**, 4061.
52. G. P. López, D. G. Castner, B. D. Ratner, *Surface and Interface Analysis*, 1991, **17**, 267.
53. J. F. Moulder, W. F. Stickle, P. E. Sobol, K. D. Bomben, *Handbook of X-ray Photoelectron Spectroscopy*, Perkin-Elmer Corporation, Eden Prairie MN, 1992.
54. L. Diederich, P. Aebi, O. M. Küttel, L. Schlapbach, *Surface Science*, 1999, **424**, L314.
55. M. Kwoka, L. Ottaviano, M. Passacantando, S. Santucci, G. Czempik, J. Szuber, *Thin Solid Films*, 2006, **490**, 36.
56. F. A. M. Koeck, R. J. Nemanich, A. Lazea, K. Haenen, *Diamond & Related Materials*, 2009, **18**, 789.
57. A. Croot, G. Wan, A. Rowan, H. D. Andrade, J. A. Smith, N. A. Fox, *Frontiers in Mechanical Engineering*, 2017, **3**, 1.
58. T. Tachibana, B. E. Williams, J. T. Glass, *Physical Review B*, 1992, **45**, 11 975.
59. C. Oshima, M. Aono, T. Tanaka, S. Kawai, *Surface Science*, 1981, **102**, 312.
60. M. Liao, Y. Koide, *Applied Physics Letters*, 2005, **87**, 022105.